Purely irrotational theories for the viscous effects on the oscillations of drops and bubbles

J.C. Padrino, T. Funada, D.D. Joseph

May, 2006

Abstract

Two purely irrotational theories of the motion of viscous fluids, viscous potential flow (VPF) and a viscous correction of viscous potential flow (VCVPF), have recently been applied to study capillary instability and to obtain the rate of decay of free gravity waves. The results from these analyses are, in general, in good to excellent agreement with exact solutions. Furthermore, the application of the dissipation method to these problems gives the same results as VCVPF. In this paper, we apply the VPF and VCVPF approximations as well as the dissipation method to the problem of the decay of waves on spheres. We treat the problem of the decay of small disturbances on a viscous drop surrounded by gas of negligible density and viscosity and a bubble immersed in a viscous liquid. The instantaneous velocity field in the viscous liquid is assumed to be irrotational. The linearized governing equations are solved by normal modes. The dissipation method applied to this problem gives rise to the same dispersion relation as VCVPF. Detailed comparisons of the eigenvalues from VPF and VCVPF and the exact solution are presented. Good agreement with the exact solution for the two purely irrotational solutions is demonstrated.

Keywords: drops, bubbles, potential flow, two-phase flow, gas-liquid flow, viscous potential flow.

1 Introduction

A viscous liquid drop surrounded by a quiescent gas or a gas bubble immersed in a viscous liquid tends to an equilibrium spherical shape if the effects of surface tension are significantly large in comparison with gravitational effects. When the spherical interface of the bubble or drop is slightly perturbed by an external agent, the bubble or drop will recover their original spherical configuration through an oscillatory motion of decreasing amplitude. In the case of the drop, depending upon its size and physical properties, the return to the spherical shape may consist of monotonically decaying standing waves. For a drop immersed in another viscous liquid, decaying oscillatory waves always occurs at the liquid-liquid interface.

Early studies on the subject for inviscid liquids are due to Kelvin (1890) and Rayleigh (1896). The former obtained an expression for the frequencies of small oscillations of an inviscid liquid globe that tends to the spherical shape by the existence of an internal gravitational potential in the absence of surface tension. The latter included surface tension instead of gravitation. Lamb (1881, 1932) considered the effect of viscosity on the rate of decay of the oscillations of a liquid globe assuming an irrotational velocity field using the dissipation method. Lamb's result is independent of the nature of the forces that drive the interface to the spherical shape. Chandrasekhar (1959) studied fully viscous effects on the small oscillations of a liquid globe with self-gravitation forces neglecting surface tension. The same form of the solution was also obtained by Reid (1960) when surface tension instead of self-gravitation is the force that tends to maintain the spherical shape. A good account of both solutions is presented in the treatise by Chandrasekhar (1961). Following Lamb's reasoning, Valentine, Sather & Heideger (1965) applied the dissipation method to the case of a drop surrounded by another viscous liquid.

A comprehensive analysis of viscous effects in a drop embeded in liquid was presented by Miller & Scriven (1968) who also included rheological properties of the interface. The limiting cases of a drop

in a vacuum or a bubble surrounded by a liquid were considered. However, no numerical results were given. Prosperetti (1980a) presented numerical results for the eigenvalue problem for modes $\ell = 2$ to $\ell = 6$. He showed that the spectrum is continuous when the liquid outside is unbounded. Previous studies relied on normal-modes. Prosperetti (1977, 1980b) considered the initial-value fully-viscous problem posed by small perturbations about the spherical shape of a drop or a bubble in which no 'a priori' form of the time dependence is assumed. The solution showed that the normal-mode results are recovered for large times.

Finite size disturbances have received some attention. Tsamopoulus & Brown (1983) considered the small-to-moderate-amplitude inviscid oscillations using perturbations methods. Lundgren & Mansour (1988) and Patzek *et al.* (1991) studied the inviscid problem posed by large oscillations applying the boundary-integral and the finite-element methods, respectively. Lundgren & Mansour also investigated the effect of a 'small' viscosity on drop oscillations. Basaran (1992) carried out the numerical analysis of moderate-to-large-amplitude axisymmetric oscillations of a viscous liquid drop.

In this paper, approximate solutions of the linearized problem for small departures from the spherical shape for a drop surrounded by a gas of negligible density and viscosity or a bubble embedded in a liquid are sought using viscous potential flow (VPF) and viscous correction of viscous potential flow (VCVPF). VPF is a purely-irrotational-flow theory in which viscosity enters through the viscous normal stresses at the the interface (Joseph & Liao 1994a, 1994b, Joseph 2003). If the viscosities of the fluids are neglected, and only the irrotational pressure and capillary forces are included in the balance at the interface, the analysis reduces to inviscid potential flow (IPF). In general, the potential flow cannot satisfy the zero-shear-stress condition at a gas-liquid interface or the continuity of the tangential velocity and shear stress at a liquid-liquid interface. Joseph & Wang (2004) proposed a formulation that adds a viscous pressure correction to VPF. This correction compensates for the discrepancy between the non-zero irrotational shear stress and the actual zero-shear-stress condition at the interface 'in the mean. The pressure correction is induced in a boundary layer which is not studied or needed in the analysis. Alternatively, a viscous correction of VPF can be obtained by applying the dissipation method (Joseph & Wang 2004). In this approximation, which requires the evaluation of the mechanical energy equation, no pressure correction is assumed and viscous effects are accounted for through the computation of the viscous dissipation originated by the irrotational flow. The dissipation method was used by Lamb (1932) in his analysis of the effect of viscosity on the decay of free gravity waves.

Funada & Joseph (2002) used VPF to study the problem of capillary instability. Their results were in much better agreement with Tomotika's (1935) exact normal-mode solution than with inviscid potential flow. Wang, Joseph & Funada (2005a) computed the growth rates for this configuration from VCVPF, when either the interior or exterior fluid is a gas of negligible density and viscosity. They found excellent agreement between their results and the exact solution. The case of capillary instability of two viscous liquids was considered by Wang, Joseph & Funada (2005b), obtaining good to reasonable conformity for the maximum growth rates whereas poor agreement for long waves. In addition, Wang *et al.* (2005a, 2005b) obtained the same eigenvalue relations as VCVPF for standing waves which decay monotonically using the dissipation method instead. The decay of free gravity waves modeled as small disturbances about an infinite plane free surface was studied by Joseph & Wang (2004) and Wang & Joseph (2006) using VPF and VCVPF. Their results were in remarkable good agreement with Lamb's exact solution for all wave numbers excluding a small interval around a critical value where waves change from progressive waves to standing ones. Moreover, the damping rate computed from VCVPF for long waves coincides with Lamb's dissipation result and exact solution. On the other hand, their result from VPF for the rate of decay agrees with Lamb's exact solution for short waves. A comprehensive review of the evolution of the theory of irrotational flow of viscous

fluids is provided in the historical notes by Joseph (2006).

Five analytical methods are thus used in this study to determine the rate of decay and frequency of the oscillations on drops and bubbles, namely,

VPF or viscous potential flow, in which the viscosity enters the analysis through the viscous normal stress at the interface.

VCVPF or viscous correction of viscous potential flow.

IPF or inviscid potential flow, in which the viscosity is set equal to zero.

Dissipation method, which requires the integration of the mechanical energy equation for irrotational motion.

Exact solution of the linearized incompressible Navier–Stokes equations.

This paper is organized as follows: First, a VPF analysis of a drop is presented; then, the pressure correction extension of VPF is described; The results of studies using VPF and VCVPF for a single spherical bubble are summarized in §4. In §5, the exact solution of the linearized fully viscous problem is reviewed. The dissipation method is applied to the spherical configuration in §6, followed by a brief discussion on the decay of waves on a plane interface with surface tension effects in §7. Results are discussed in §8 where several final remarks are presented.

2 VPF analysis of a single spherical drop immersed in another fluid – More viscous fluid within the drop

Consider a single spherical drop of radius a filled with a fluid with density ρ_l and viscosity μ_l immersed in another fluid with density ρ_a and viscosity μ_a. The coefficient of interfacial tension is denoted as γ. Both fluids are incompressible and Newtonian with gravity neglected. At the basic or undisturbed state both fluids are at rest. For convenience, we shall first consider the case when drop is more viscous, $\mu_l \geq \mu_a$.

When the basic state is disturbed with small-irrotational perturbations, the resulting velocity field can be written in terms of a velocity potential $\boldsymbol{u}^* = \boldsymbol{\nabla}\phi^*$. Since $\boldsymbol{\nabla}\cdot\boldsymbol{u}^* = 0$, we have

$$\nabla^2\phi_l^* = 0 \qquad 0 \leq r < a+\zeta, \tag{2.1}$$

$$\nabla^2\phi_a^* = 0 \qquad a+\zeta < r < \infty, \tag{2.2}$$

for the interior and exterior fluid motion, respectively. The disturbance of the spherical interface is denoted by $\zeta \equiv \zeta(t,\theta,\varphi)$; the interface position is $r = a+\zeta$.

For irrotational flow the incompressible Navier–Stokes equations reduce to the Bernoulli equation. For the fluid within the drop

$$\frac{\partial\phi_l^*}{\partial t} + \frac{|\boldsymbol{\nabla}\phi_l^*|^2}{2} + \frac{p_l^*}{\rho_l} = B_l \qquad 0 \leq r < a+\zeta, \tag{2.3}$$

and, for the exterior fluid,

$$\frac{\partial\phi_a^*}{\partial t} + \frac{|\boldsymbol{\nabla}\phi_a^*|^2}{2} + \frac{p_a^*}{\rho_a} = B_a \qquad a+\zeta < r < \infty, \tag{2.4}$$

where ϕ^* is the velocity potential and p^* is the pressure of the disturbed motion; B_l and B_a are constants. The pressure disturbance p has been added to the pressure of the basic state P, such that $p^* = P + p$. Furthermore, we have $\phi^* = \phi$. The boundary conditions at $r = a + \zeta$ are given by the continuity of the normal velocity

$$[[\boldsymbol{u}^* \cdot \boldsymbol{n}]] = 0, \tag{2.5}$$

and the balance of the normal stress discontinuity across the interface by the interfacial tension

$$[[-p^* + 2\mu \boldsymbol{n} \cdot \boldsymbol{\nabla} \boldsymbol{u}^* \cdot \boldsymbol{n}]] = \gamma \boldsymbol{\nabla} \cdot \boldsymbol{n}, \tag{2.6}$$

where $\boldsymbol{n}$ is the outward unit normal from fluid l. The notation $[[\cdot]] = (\cdot)_{r=b^+} - (\cdot)_{r=b^-}$ is being used to denote the jump across the generic interface located at $r = b$. The outward unit normal vector can be obtained from

$$\boldsymbol{n} = \frac{1}{|\boldsymbol{N}|}\left[\boldsymbol{e}_r - \boldsymbol{e}_\theta \frac{1}{r}\frac{\partial \zeta}{\partial \theta} - \boldsymbol{e}_\varphi \frac{1}{r\sin\theta}\frac{\partial \zeta}{\partial \varphi}\right], \tag{2.7}$$

$$|\boldsymbol{N}| = \sqrt{1 + \left(\frac{1}{r}\frac{\partial \zeta}{\partial \theta}\right)^2 + \left(\frac{1}{r\sin\theta}\frac{\partial \zeta}{\partial \varphi}\right)^2}, \tag{2.8}$$

at $r = a + \zeta$. Moreover, the following kinematic condition must be satisfied at $r = a + \zeta$

$$u_r^* = \frac{D\zeta}{Dt} = \frac{\partial \zeta}{\partial t} + \boldsymbol{u}^* \cdot \boldsymbol{\nabla} \zeta. \tag{2.9}$$

With regard to the basic state, the undisturbed pressure must satisfy,

$$\frac{P_l}{\rho_l} = B_l \qquad 0 \le r < a, \tag{2.10}$$

$$\frac{P_a}{\rho_a} = B_a \qquad a < r < \infty, \tag{2.11}$$

while the normal stress jump at the interface is balance by the surface tension as

$$P_l - P_a = \frac{2\gamma}{a}, \tag{2.12}$$

at $r = a$ for the undisturbed state.

After subtracting the basic state in (2.10) and (2.11) from the disturbed fluid motion given in (2.1), (2.2),(2.3) and (2.4) and performing standard linearization of the resulting expressions by neglecting products of the small fluctuations and products of their derivatives, one obtains, for the interior motion $(0 \le r < a)$,

$$\nabla^2 \phi_l = 0, \tag{2.13}$$

$$p_l = -\rho_l \frac{\partial \phi_l}{\partial t}, \tag{2.14}$$

and, for the exterior motion $(a < r < \infty)$,

$$\nabla^2 \phi_a = 0, \tag{2.15}$$

$$p_a = -\rho_a \frac{\partial \phi_a}{\partial t}. \tag{2.16}$$

The boundary conditions (2.5), (2.6) and (2.9) are also linearized, yielding, at $r = a$,

$$u_{r,l} = u_{r,a} \tag{2.17}$$

$$\left[\left[-p + 2\mu \frac{\partial u_r}{\partial r}\right]\right] = \frac{\gamma}{a^2}(L^2 - 2)\zeta, \tag{2.18}$$

$$u_r = \frac{\partial \zeta}{\partial t}, \tag{2.19}$$

with, $u_r = \partial\phi/\partial r$. The operator L^2 is also known as the spherical Laplacian and emerges, for instance, in the solution of the Laplace equation using spherical coordinates by applying the method of separation of variables. It is defined as

$$-L^2\zeta = \frac{1}{\sin\theta}\frac{\partial}{\partial\theta}\left(\sin\theta\frac{\partial\zeta}{\partial\theta}\right) + \frac{1}{\sin^2\theta}\frac{\partial^2\zeta}{\partial\varphi^2}. \tag{2.20}$$

Solutions of (2.13) and (2.15) for the interior and exterior of a sphere, respectively, can be sought in the form

$$\phi_l(r,\theta,\varphi,t) = \sum_{\ell=0}^{\infty} A_\ell \left(\frac{r}{a}\right)^\ell e^{-\sigma_\ell t} S_\ell(\theta,\varphi) + \text{c.c.} \qquad 0 \le r < a, \tag{2.21}$$

$$\phi_a(r,\theta,\varphi,t) = \sum_{\ell=0}^{\infty} C_\ell \left(\frac{r}{a}\right)^{-\ell-1} e^{-\sigma_\ell t} S_\ell(\theta,\varphi) + \text{c.c.} \qquad a < r < \infty, \tag{2.22}$$

such that ϕ_l is finite at $r = 0$ and ϕ_a vanishes in the limit $r \to \infty$; σ_ℓ is an eigenvalue to be determined. It will be shown that σ_ℓ does not depend upon the index m. The symbol c.c. designates the complex conjugate of the previous term. The functions S_ℓ are the surface harmonics of integral order

$$S_\ell(\theta,\varphi) = \sum_{m=-\ell}^{\ell} B_{\ell m} Y_\ell^m(\theta,\varphi), \tag{2.23}$$

which, with the choice $\bar{B}_{\ell m} = B_{\ell,-m}$, are real functions. The functions $Y_\ell^m(\theta,\varphi)$ are known as the spherical harmonics (Strauss, 1992)

$$Y_\ell^m(\theta,\varphi) = P_\ell^{|m|}(\cos\theta)e^{im\varphi}, \tag{2.24}$$

where $P_\ell^{|m|}$ are the associated Legendre functions. The spherical harmonics satisfy

$$L^2 Y_\ell^m(\theta,\varphi) = \ell(\ell+1)Y_\ell^m(\theta,\varphi), \tag{2.25}$$

for $\ell = 0, 1, 2, \ldots$ and $m = -\ell, \ldots, -1, 0, 1, \ldots, \ell$. The operator L^2 has been defined in (2.20). Expressions for the radial components of the velocity can be obtained from (2.21) and (2.22) by applying $u_r = \partial\phi/\partial r$,

$$u_{r,l}(r,\theta,\varphi,t) = \sum_{\ell=0}^{\infty} A_\ell \frac{\ell}{a^\ell} r^{\ell-1} \mathrm{e}^{-\sigma_\ell t} S_\ell + \text{c.c.}, \tag{2.26}$$

$$u_{r,a}(r,\theta,\varphi,t) = \sum_{\ell=0}^{\infty} -C_\ell \frac{\ell+1}{a^{-\ell-1}} r^{-\ell-2} \mathrm{e}^{-\sigma_\ell t} S_\ell + \text{c.c.}. \tag{2.27}$$

After replacing expressions (2.21) and (2.22) for ϕ_l and ϕ_a, respectively, into (2.14) and (2.16), the pressure disturbances become

$$p_l(r,\theta,\varphi,t) = \sum_{\ell=0}^{\infty} \rho_l \sigma_\ell A_\ell \left(\frac{r}{a}\right)^{\ell} \mathrm{e}^{-\sigma_\ell t} S_\ell(\theta,\varphi) + \text{c.c.} \qquad 0 \le r < a, \tag{2.28}$$

$$p_a(r,\theta,\varphi,t) = \sum_{\ell=0}^{\infty} \rho_a \sigma_\ell C_\ell \left(\frac{r}{a}\right)^{-\ell-1} \mathrm{e}^{-\sigma_\ell t} S_\ell(\theta,\varphi) + \text{c.c.} \qquad a < r < \infty. \tag{2.29}$$

Let us write the disturbance of the spherical shape of the interface as a series expansion,

$$\zeta(\theta,\varphi,t) = \sum_{\ell=0}^{\infty} \zeta_\ell(\theta,\varphi) \mathrm{e}^{-\sigma_\ell t} + \text{c.c.}. \tag{2.30}$$

Substitution of (2.26),(2.27) and (2.30) into the boundary conditions (2.17) and (2.19) yields

$$-\sigma_\ell \zeta_\ell = \left(\frac{\ell}{a}\right) A_\ell S_\ell, \qquad \sigma_\ell \zeta_\ell = \left(\frac{\ell+1}{a}\right) C_\ell S_\ell. \tag{2.31}$$

By considering $\zeta_\ell(\theta,\varphi) = \zeta_{0\ell} S_\ell(\theta,\varphi)$, where $\zeta_{0\ell}$ is a constant, expression (2.31) becomes

$$-\sigma_\ell \zeta_{0\ell} = \left(\frac{\ell}{a}\right) A_\ell, \qquad \sigma_\ell \zeta_{0\ell} = \left(\frac{\ell+1}{a}\right) C_\ell. \tag{2.32}$$

We have

$$(L^2-2)\zeta = \sum_{\ell=0}^{\infty} \{\ell(\ell+1)-2\} \zeta_{0\ell} \mathrm{e}^{-\sigma_\ell t} S_\ell + \text{c.c.} = \sum_{\ell=0}^{\infty} (\ell+2)(\ell-1) \zeta_{0\ell} \mathrm{e}^{-\sigma_\ell t} S_\ell + \text{c.c.}, \tag{2.33}$$

by virtue of (2.25) and (2.30). Substitution of (2.26), (2.27), (2.28) and (2.29) into the R.H.S. of (2.18), using the result (2.33) and replacing A_ℓ and C_ℓ with (2.32) yields the dispersion relation for the eigenvalue σ_ℓ, which after some manipulation, may be written as

$$\begin{aligned} \left(\rho_l(\ell+1)+\rho_a\ell\right)\sigma_\ell^2 \quad &- \quad \left(\frac{2\mu_l}{a^2}(\ell+1)\ell(\ell-1) + \frac{2\mu_a}{a^2}(\ell+2)(\ell+1)\ell\right)\sigma_\ell \\ &+ \quad \frac{\gamma}{a^3}(\ell+2)(\ell+1)\ell(\ell-1) = 0, \end{aligned} \tag{2.34}$$

for $\ell = 0, 1, 2, \ldots$. This quadratic equation can be solved yielding,

$$\begin{aligned} \sigma \quad = \quad & \frac{\mu_l(\ell+1)\ell(\ell-1) + \mu_a(\ell+2)(\ell+1)\ell}{a^2\left(\rho_l(\ell+1)+\rho_a\ell\right)} \\ & \pm \sqrt{\left[\frac{\mu_l(\ell+1)\ell(\ell-1) + \mu_a(\ell+2)(\ell+1)\ell}{a^2\left(\rho_l(\ell+1)+\rho_a\ell\right)}\right]^2 - \frac{\gamma}{a^3}\frac{(\ell+2)(\ell+1)\ell(\ell-1)}{\rho_l(\ell+1)+\rho_a\ell}}, \end{aligned} \tag{2.35}$$

where the subscript ℓ has been dropped from σ for convenience. Expressions (2.34) and (2.35) may be written in dimensionless form with the following choices of dimensionless parameters (Funada & Joseph, 2002),

$$\hat{l} = \frac{\rho_a}{\rho_l}, \quad \hat{m} = \frac{\mu_a}{\mu_l}, \quad \hat{\sigma} = \sigma\frac{a}{U} \qquad \text{with} \qquad U = \sqrt{\frac{\gamma}{\rho_l a}}, \tag{2.36}$$

In dimensionless form, expression (2.34) becomes,

$$\left((\ell+1)+\hat{l}\ell\right)\hat{\sigma}_\ell^2 - \frac{2}{\sqrt{J}}\left((\ell+1)\ell(\ell-1)+\hat{m}(\ell+2)(\ell+1)\ell\right)\hat{\sigma} + (\ell+2)(\ell+1)\ell(\ell-1) = 0 \tag{2.37}$$

with a Reynolds number

$$J = \frac{\rho_l V a}{\mu_l} = Oh^2 \qquad \text{with} \qquad V = \frac{\gamma}{\mu_l}, \tag{2.38}$$

where ρ_l and μ_l refers to the density and viscosity of the more viscous fluid and Oh is the Ohnesorge number. Therefore, the eigenvalue $\hat{\sigma}$ for viscous potential flow (VPF) can be computed from

$$\begin{aligned}\hat{\sigma} &= \frac{(\ell+1)\ell(\ell-1)+\hat{m}(\ell+2)(\ell+1)\ell}{\sqrt{J}\left((\ell+1)+\hat{l}\ell\right)} \\ &\pm \sqrt{\left[\frac{(\ell+1)\ell(\ell-1)+\hat{m}(\ell+2)(\ell+1)\ell}{\sqrt{J}((\ell+1)+\hat{l}\ell)}\right]^2 - \frac{(\ell+2)(\ell+1)\ell(\ell-1)}{(\ell+1)+\hat{l}\ell}},\end{aligned} \tag{2.39}$$

which has two different real roots or two complex roots can. In the former case, the interface does not oscillate and the disturbances are damped. In the later case, $\hat{\sigma} = \hat{\sigma}_R \pm i\hat{\sigma}_I$ where the real part represents the damping coefficient while the imaginary part corresponds to the frequency of the damped oscillations.

If the external fluid has negligible density and viscosity ($\hat{l} \to 0$ and $\hat{m} \to 0$), expression (2.39) becomes,

$$\hat{\sigma} = \frac{\ell(\ell-1)}{\sqrt{J}} \pm \sqrt{\left[\frac{\ell(\ell-1)}{\sqrt{J}}\right]^2 - (\ell+2)\ell(\ell-1)}, \tag{2.40}$$

which, in dimensional form, can be written as

$$\sigma = \frac{\nu}{a^2}\ell(\ell-1) \pm \sqrt{\left[\frac{\nu}{a^2}\ell(\ell-1)\right]^2 - \frac{\gamma}{\rho a^3}(\ell+2)\ell(\ell-1)}. \tag{2.41}$$

Moreover, for an inviscid drop $\sqrt{J} \to \infty$ and (2.40) reduces to

$$\hat{\sigma}_D = \pm i\sqrt{(\ell+2)\ell(\ell-1)} = \pm i\hat{\sigma}_D^* \qquad \text{or} \qquad \sigma_D = \pm i\sqrt{\frac{\gamma}{\rho a^3}(\ell+2)\ell(\ell-1)} = \pm i\sigma_D^*, \tag{2.42}$$

in dimensional form and the drop oscillates about the spherical form. The density of the drop is denoted by ρ. This result was obtained by Lamb (1932), p. 475.

When both fluids are considered inviscid (IPF), expression (2.39) simplifies to ($\hat{m} \to 0$ and $\sqrt{J} \to \infty$)

$$\hat{\sigma} = \pm i\sqrt{\frac{(\ell+2)(\ell+1)\ell(\ell-1)}{(\ell+1)+\hat{l}\ell}} \qquad \text{or} \qquad \sigma = \pm i\sqrt{\frac{\gamma}{a^3}\frac{(\ell+2)(\ell+1)\ell(\ell-1)}{\rho_l(\ell+1)+\rho_a\ell}}. \tag{2.43}$$

Again, the same expression found by Lamb (1932).

From the expression obtained from VPF in (2.40), one can readily find two roots for the rate of decay as $J \to 0$ in the drop. The relevant root on physical grounds is given by

$$\hat{\sigma} = \hat{\sigma}_D^{*2}\sqrt{J}\frac{1}{2\ell(\ell-1)} \qquad \text{or} \qquad \sigma = \sigma_D^{*2}\frac{a^2}{\nu}\frac{1}{2\ell(\ell-1)} \tag{2.44}$$

where the last expression is in dimensional form. In the case $J \to \infty$ (low viscosity, say), the eigenvalues are complex, and then one encounters progressive decaying waves. These eigenvalues behave as

$$\hat{\sigma} = \frac{\ell(\ell-1)}{\sqrt{J}} \pm i\hat{\sigma}_D^* \qquad \text{or} \qquad \sigma = \frac{\nu}{a^2}\ell(\ell-1) \pm i\sigma_D^*. \tag{2.45}$$

3 Pressure correction for VPF – Single spherical drop surrounded by gas

Let us consider the case where the exterior fluid is a gas of negligible viscosity and density. Assuming that the interior fluid is irrotational, the shear stress at the free surface of the sphere violates the zero-shear-stress condition. Following Joseph and Wang (2004), a pressure correction p^v can be added to the irrotational pressure in order to compensate for this discontinuity. They showed that the power of the pressure correction p^v equals the power of the irrotational shear stress

$$\int_A (-p^v) u_n \mathrm{d}A = \int_A \tau_s u_s \mathrm{d}A \tag{3.1}$$

and p^v is a harmonic function, such that

$$\nabla^2 p^v = 0. \tag{3.2}$$

For the interior of a sphere of radius a, the following expression solves (3.2)

$$-p^v = \sum_{k=0}^{\infty} D_k \left(\frac{r}{a}\right)^k e^{-\sigma_k t} S_k(\theta,\varphi) + \text{c.c.}, \tag{3.3}$$

where D_k are constants. The balance of the normal stress at the sphere's interface $r = a$ is modified by adding p^v

$$-(p+p^v) + 2\mu\frac{\partial^2\phi}{\partial r^2} = -\frac{\gamma}{a^2}\left(L^2-2\right)\zeta, \tag{3.4}$$

where the subscript l has been dropped for convenience. Substitution of the solution for p^v (3.3) and using (2.21), (2.28) and (2.33) yields,

$$\rho A_\ell \sigma_\ell^2 - \left[D_\ell + \frac{2\mu}{a^2}\ell(\ell-1)A_\ell\right]\sigma_\ell = -\frac{\gamma}{a^3}(\ell+2)\ell(\ell-1)A_\ell, \tag{3.5}$$

where the orthogonality property of the spherical harmonics has been used. For a sphere of radius a the integrals in (3.1) can be written in terms of the velocity and shear stress components

$$\int_A (-p^v) u_r \mathrm{d}A = \int_A \left(\tau_{r\theta}u_\theta + \tau_{r\varphi}u_\varphi\right)\mathrm{d}A. \tag{3.6}$$

The velocity components can be computed from

$$u_r = \frac{\partial \phi}{\partial r}, \qquad u_\theta = \frac{1}{r}\frac{\partial \phi}{\partial \theta}, \qquad u_\varphi = \frac{1}{r\sin\theta}\frac{\partial \phi}{\partial \varphi}, \tag{3.7}$$

and the shear stress components from

$$\begin{aligned} \tau_{r\theta} &= \mu\left(\frac{\partial u_\theta}{\partial r} - \frac{u_\theta}{r} + \frac{1}{r}\frac{\partial u_r}{\partial \theta}\right) = \frac{2\mu}{r}\left(\frac{\partial^2 \phi}{\partial r \partial \theta} - \frac{1}{r}\frac{\partial \phi}{\partial \theta}\right) \\ \tau_{r\varphi} &= \mu\left(\frac{1}{r\sin\theta}\frac{\partial u_r}{\partial \varphi} + \frac{\partial u_\varphi}{\partial r} - \frac{u_\varphi}{r}\right) = \frac{2\mu}{r\sin\theta}\left(\frac{\partial^2 \phi}{\partial r \partial \varphi} - \frac{1}{r}\frac{\partial \phi}{\partial \varphi}\right) \end{aligned} \tag{3.8}$$

Therefore, for the velocity potential defined in (2.21), the velocity components on the surface of the sphere $r = a$ become,

$$u_r = \sum_{\ell=0}^{\infty} A_\ell \frac{\ell}{a} e^{-\sigma_\ell t} S_\ell + \text{c.c.}, \quad u_\theta = \sum_{\ell=0}^{\infty} \frac{A_\ell}{a} e^{-\sigma_\ell t}\frac{\partial S_\ell}{\partial \theta} + \text{c.c.}, \quad u_\varphi = \sum_{\ell=0}^{\infty} \frac{A_\ell}{a\sin\theta} e^{-\sigma_\ell t}\frac{\partial S_\ell}{\partial \varphi} + \text{c.c.}, \tag{3.9}$$

and the shear stress components are

$$\tau_{r\theta} = \sum_{\ell=0}^{\infty} 2\mu \frac{A_\ell}{a^2}(\ell - 1) e^{-\sigma_\ell t}\frac{\partial S_\ell}{\partial \theta} + \text{c.c.}, \qquad \tau_{r\varphi} = \sum_{\ell=0}^{\infty} 2\mu \frac{A_\ell}{a^2 \sin\theta}(\ell - 1) e^{-\sigma_\ell t}\frac{\partial S_\ell}{\partial \varphi} + \text{c.c.} \tag{3.10}$$

The left hand side of (3.6) then becomes,

$$\int_A (-p^v) u_r \, \mathrm{d}A = 2\,\mathrm{Re}\left[\sum_{\ell=0}^{\infty}\sum_{k=0}^{\infty} a^2 D_\ell e^{-\sigma_\ell t}\left(\frac{k}{a}\right)\left(A_k e^{-\sigma_k t} + \bar{A}_k e^{-\bar{\sigma}_k t}\right)\int_0^{2\pi}\int_0^{\pi} S_\ell S_k \sin\theta \mathrm{d}\theta \mathrm{d}\varphi\right], \tag{3.11}$$

where $\mathrm{Re}[z]$ delivers the real part of a complex number z. The equality in (3.11) follows from the formula presented in the Appendix, which is also used in the integration of the right hand side of (3.6) and similar integrals in §4 and §6. Using the definition of S_n in (2.23), the double integral in (3.11) can be written as

$$\int_0^{2\pi}\int_0^{\pi} S_\ell S_k \sin\theta \mathrm{d}\theta \mathrm{d}\varphi = \sum_{m=-\ell}^{\ell}\sum_{j=-k}^{k} B_{\ell m}\bar{B}_{kj}\int_0^{2\pi}\int_0^{\pi} P_\ell^{|m|}(\cos\theta) P_k^{|j|}(\cos\theta) e^{i(m-j)\varphi}\sin\theta \mathrm{d}\theta \mathrm{d}\varphi, \tag{3.12}$$

since S_k is real (i.e. $S_k = \bar{S}_k$). This integral is zero for all the different duplets $(\ell, m) \neq (k, j)$. Then, we are left with,

$$\begin{aligned} \int_0^{2\pi}\int_0^{\pi} [S_\ell(\theta,\varphi)]^2 \sin\theta \mathrm{d}\theta \mathrm{d}\varphi &= \sum_{m=0}^{\ell} 2\pi F_{\ell m}\int_0^{\pi} [P_\ell^m(\cos\theta)]^2 \sin\theta \mathrm{d}\theta \\ &= \sum_{m=0}^{\ell} F_{\ell m}\left[\frac{4\pi}{2\ell+1}\frac{(\ell+m)!}{(\ell-m)!}\right], \end{aligned} \tag{3.13}$$

using a standard result for the integral in the second term. Here, $F_{\ell m}$ represent real constants. Then, from (3.11) the power of the pressure correction can be expressed as

$$\int_A (-p^v) u_r \mathrm{d}A = 2\,\mathrm{Re}\left[\sum_{\ell=0}^{\infty}\sum_{m=0}^{\ell} F_{\ell m} 4\pi a D_\ell e^{-\sigma_\ell t}(A_\ell e^{-\sigma_\ell t} + \bar{A}_\ell e^{-\bar{\sigma}_\ell t})\frac{\ell}{2\ell+1}\frac{(\ell+m)!}{(\ell-m)!}\right]. \tag{3.14}$$

Similarly, the right hand side of (3.6) yields,

$$\int_A (\tau_{r\theta}u_\theta + \tau_{r\varphi}u_\varphi)\,\mathrm{d}A = 2\mathrm{Re}\Bigg[\sum_{\ell=0}^{\infty}\sum_{k=0}^{\infty}\frac{2\mu}{a}A_\ell e^{-\sigma_\ell t}(\ell-1)(A_k e^{-\sigma_k t}+\bar{A}_k e^{-\bar{\sigma}_k t}) \int_0^{2\pi}\int_0^{\pi}\left(\sin\theta\frac{\partial S_\ell}{\partial\theta}\frac{\partial S_k}{\partial\theta}+\frac{1}{\sin\theta}\frac{\partial S_\ell}{\partial\varphi}\frac{\partial S_k}{\partial\varphi}\right)\mathrm{d}\theta\mathrm{d}\varphi\Bigg]. \tag{3.15}$$

The integral in (3.15) gives rise to

$$\int_0^{2\pi}\int_0^{\pi}\left[\sin\theta\frac{\partial S_\ell}{\partial\theta}\frac{\partial S_k}{\partial\theta}+\frac{1}{\sin\theta}\frac{\partial S_\ell}{\partial\varphi}\frac{\partial S_k}{\partial\varphi}\right]\mathrm{d}\theta\mathrm{d}\varphi = \sum_{m=-\ell}^{\ell}\sum_{j=-k}^{k}B_{\ell m}\bar{B}_{kj}$$

$$\int_0^{2\pi}\int_0^{\pi}\left[\sin\theta\frac{dP_\ell^{|m|}(\chi)}{d\theta}\frac{dP_k^{|j|}(\chi)}{d\theta}+\frac{mj}{\sin\theta}P_\ell^{|m|}(\chi)P_k^{|j|}(\chi)\right]e^{i(m-j)\varphi}\mathrm{d}\theta\mathrm{d}\varphi, \tag{3.16}$$

where $\chi = \cos\theta$. This integral is also zero for all different duplets $(n,m) \neq (k,j)$. Otherwise, this integral reduces to (Bowman, Senior & Uslenghi 1987; Moriguchi, Udagawa & Hitotsumatsu 1999)

$$\begin{aligned}
&\int_0^{2\pi}\int_0^{\pi}\left[\sin\theta\left(\frac{\partial S_\ell}{\partial\theta}\right)^2+\frac{1}{\sin\theta}\left(\frac{\partial S_\ell}{\partial\varphi}\right)^2\right]\mathrm{d}\theta\mathrm{d}\varphi = \\
&= \sum_{m=0}^{\ell}2\pi F_{\ell m}\int_0^{\pi}\left[\sin\theta\left(\frac{dP_\ell^m(\chi)}{d\theta}\right)^2+\frac{m^2}{\sin\theta}\left(P_\ell^m(\chi)\right)^2\right]\mathrm{d}\theta \\
&= \sum_{m=0}^{\ell}F_{\ell m}\left[\frac{4\pi\ell(\ell+1)}{(2\ell+1)}\frac{(\ell+m)!}{(\ell-m)!}\right].
\end{aligned} \tag{3.17}$$

Therefore, we have found that the power of the shear stress can be expressed as

$$\begin{aligned}
\int_A(\tau_{r\theta}u_\theta+\tau_{r\varphi}u_\varphi)\mathrm{d}A &= 2\,\mathrm{Re}\Bigg[\sum_{\ell=0}^{\infty}\sum_{m=0}^{\ell}F_{\ell m}8\pi\mu\frac{A_\ell}{a}e^{-\sigma_\ell t}(A_\ell e^{-\sigma_\ell t}+ \\
&+ \bar{A}_\ell e^{-\bar{\sigma}_\ell t})\frac{\ell(\ell+1)(\ell-1)}{(2\ell+1)}\frac{(\ell+m)!}{(\ell-m)!}\Bigg].
\end{aligned} \tag{3.18}$$

By virtue of (3.6), equating (3.14) and (3.18) yields the relation

$$D_\ell = 2\mu\frac{A_\ell}{a^2}(\ell+1)(\ell-1). \tag{3.19}$$

Replacing D_ℓ in (3.19) in (3.5) yields the dispersion relation for the complex eigenvalue σ_ℓ arising from VCVPF (again we drop the subscript ℓ for convenience),

$$\sigma^2 - \frac{2\nu}{a^2}(2\ell+1)(\ell-1)\sigma + \frac{\gamma}{\rho a^3}(\ell+2)\ell(\ell-1) = 0, \tag{3.20}$$

with roots,

$$\sigma = \frac{\nu}{a^2}(2\ell+1)(\ell-1) \pm \sqrt{\left[\frac{\nu}{a^2}(2\ell+1)(\ell-1)\right]^2 - \frac{\gamma}{\rho a^3}(\ell+2)\ell(\ell-1)}. \tag{3.21}$$

In the case of progressive waves, the rate of decay $(\nu/a^2)(2\ell+1)(\ell-1)$ was obtained by Lamb (1932) in §355 through the dissipation method. In the present calculations, the relation (3.21) gives the decay rate of progressive waves ($\mathrm{Im}(\sigma) \neq 0$) as well as the wave velocity. For $\mathrm{Im}(\sigma) = 0$, the monotonically decay rate for standing waves including the effect of surface tension is obtained. Expression (3.21) can be compared with results in (2.41) and (2.42) from VPF and IPF, respectively.

In dimensionless form, the dispersion relation for VCVPF (3.21) can be written as,

$$\hat{\sigma} = \frac{(2\ell+1)(\ell-1)}{\sqrt{J}} \pm \sqrt{\left[\frac{(2\ell+1)(\ell-1)}{\sqrt{J}}\right]^2 - (\ell+2)\ell(\ell-1)}, \tag{3.22}$$

where the dimensionless parameter $\hat{\sigma}$ and the Reynolds number J have been defined in (2.36) and (2.38), respectively. Expression (3.22) can be compared with (2.40) from VPF and (2.42) from IPF.

As $J \to 0$, VCVPF produces two roots for the rate of decay from (3.21), the following giving the lowest decay rate,

$$\hat{\sigma} = \hat{\sigma}_D^{*2}\sqrt{J}\frac{1}{2(2\ell+1)(\ell-1)} \qquad \text{or} \qquad \sigma = \sigma_D^{*2}\frac{a^2}{\nu}\frac{1}{2(2\ell+1)(\ell-1)}. \tag{3.23}$$

In the case of $J \to \infty$ the eigenvalues are complex,

$$\hat{\sigma} = \frac{(2\ell+1)(\ell-1)}{\sqrt{J}} \pm i\hat{\sigma}_D^* \qquad \text{or} \qquad \sigma = \frac{\nu}{a^2}(2\ell+1)(\ell-1) \pm i\sigma_D^*. \tag{3.24}$$

Hence, one finds progressive–decaying waves. The definitions of $\hat{\sigma}_D^*$ and σ_D^* are given in (2.42).

Prosperetti (1977) studied the initial value problem posed by small departures from the spherical shape of a viscous drop surrounded by another viscous liquid. In the limiting case of a drop in a vacuum, he found (3.21) in the limit $t \to 0$ if an irrotational initial condition is assumed. We remark that (3.21) was obtained here by a different method. Similarly, in the limiting case of a bubble, Prosperetti's initial-value-problem analysis with an irrotational initial condition yields, for $t \to 0$, the same dispersion relation as the one obtained from VCVPF in the next section.

4 Single spherical bubble immersed in a liquid – VPF and VCVPF analyses

The dispersion equation (2.39) also holds when the exterior fluid has a higher viscosity than the interior fluid (inverse problem). Nevertheless, in order to keep our convention $\mu_l \geq \mu_a$, we shall interchange the subscripts l and a in that expression. Then, the parameter $\hat{m} \leq 1$ and the expression for the dimensionless eigenvalue $\hat{\sigma}$ from VPF becomes

$$\begin{aligned}\hat{\sigma} &= \frac{\hat{m}(\ell+1)\ell(\ell-1) + (\ell+2)(\ell+1)\ell}{\sqrt{J}\left(\hat{l}(\ell+1)+\ell\right)} \\ &\pm \sqrt{\left[\frac{\hat{m}(\ell+1)\ell(\ell-1) + (\ell+2)(\ell+1)\ell}{\sqrt{J}(\hat{l}(\ell+1)+\ell)}\right]^2 - \frac{(\ell+2)(\ell+1)\ell(\ell-1)}{\hat{l}(\ell+1)+\ell}}.\end{aligned} \tag{4.25}$$

If the sphere represents a bubble of negligible density and viscosity ($\hat{l} \to 0$ and $\hat{m} \to 0$), (4.25) becomes

$$\hat{\sigma} = \frac{(\ell+2)(\ell+1)}{\sqrt{J}} \pm \sqrt{\left[\frac{(\ell+2)(\ell+1)}{\sqrt{J}}\right]^2 - (\ell+2)(\ell+1)(\ell-1)}, \tag{4.26}$$

for VPF. In dimensional form, expression (4.26) can be written as

$$\sigma = \frac{\nu}{a^2}(\ell+2)(\ell+1) \pm \sqrt{\left[\frac{\nu}{a^2}(\ell+2)(\ell+1)\right]^2 - \frac{\gamma}{\rho a^3}(\ell+2)(\ell+1)(\ell-1)}. \tag{4.27}$$

In the limit of an inviscid external fluid $\sqrt{J} \to \infty$ in (4.26) we obtain

$$\begin{aligned} \hat{\sigma}_B &= \pm i\sqrt{(\ell+2)(\ell+1)(\ell-1)} = \pm i\hat{\sigma}_B^* \qquad \text{or} \\ \sigma_B &= \pm i\sqrt{\frac{\gamma}{\rho a^3}(\ell+2)(\ell+1)(\ell-1)} = \pm i\sigma_B^*, \end{aligned} \tag{4.28}$$

where the last expression gives the dimensional form of the oscillation frequency and the bubble oscillates about the spherical shape without damping. This expression was obtained by Lamb (1932).

The dispersion relation from VCVPF applied to a bubble immersed in a liquid can be determined following the same steps described in the case of a drop surrounded by a fluid of negligible density and viscosity. A pressure correction is added to the pressure corresponding to the irrotational flow of a viscous fluid surrounding the bubble containing gas with zero density and viscosity. The velocity potential defined in (2.22) is used in these calculations. The analysis yields the following dispersion relation,

$$\sigma^2 - 2\frac{\nu}{a^2}(2\ell+1)(\ell+2)\sigma + \frac{\gamma}{\rho a^3}(\ell+2)(\ell+1)(\ell-1) = 0, \tag{4.29}$$

such that

$$\sigma = \frac{\nu}{a^2}(2\ell+1)(\ell+2) \pm \sqrt{\left[\frac{\nu}{a^2}(2\ell+1)(\ell+2)\right]^2 - \frac{\gamma}{\rho a^3}(\ell+2)(\ell+1)(\ell-1)}, \tag{4.30}$$

which, in dimensionless form can be written as,

$$\hat{\sigma} = \frac{(2\ell+1)(\ell+2)}{\sqrt{J}} \pm \sqrt{\left[\frac{(2\ell+1)(\ell+2)}{\sqrt{J}}\right]^2 - (\ell+2)(\ell+1)(\ell-1)}. \tag{4.31}$$

In the case of small oscillations, the rate of decay given in (4.30) as $(\nu/a^2)(2\ell+1)(\ell+2)$ is the same as the rate computed by Lamb (1932) using the dissipation method without the explicit inclusion of the surface tension effects in the formulation.

The dispersion relation obtained from VPF in (4.27) can be used to study the trend followed by the disturbances when $J \to 0$ ($\nu \to \infty$, say) in the case of the bubble. For this case, monotonically decaying waves are predicted with decay rate

$$\hat{\sigma} = \hat{\sigma}_B^{*2}\sqrt{J}\frac{1}{2(\ell+2)(\ell+1)} \qquad \text{or} \qquad \sigma = \sigma_B^{*2}\frac{a^2}{\nu}\frac{1}{2(\ell+2)(\ell+1)}, \tag{4.32}$$

while VCVPF expression (4.30) yields the following result as $J \to 0$,

$$\hat{\sigma} = \hat{\sigma}_B^{*2}\sqrt{J}\frac{1}{2(2\ell+1)(\ell+2)} \qquad \text{or} \qquad \sigma = \sigma_B^{*2}\frac{a^2}{\nu}\frac{1}{2(2\ell+1)(\ell+2)}. \tag{4.33}$$

Expressions for $\hat{\sigma}_B^*$ and σ_B^* are given in (4.28).

In the case of $J \to \infty$, VPF analysis for the bubble yields

$$\hat{\sigma} = \frac{(\ell+2)(\ell+1)}{\sqrt{J}} \pm i\hat{\sigma}_B^* \qquad \text{or} \qquad \sigma = \frac{\nu}{a^2}(\ell+2)(\ell+1) \pm i\sigma_B^*. \tag{4.34}$$

Therefore, progressive-decaying waves are found. Similarly, VCVPF predicts

$$\hat{\sigma} = \frac{(2\ell+1)(\ell+2)}{\sqrt{J}} \pm i\hat{\sigma}_B^* \qquad \text{or} \qquad \sigma = \frac{\nu}{a^2}(2\ell+1)(\ell+2) \pm i\sigma_B^*. \tag{4.35}$$

In the next section it is shown that these results from VCVPF coincide with the results obtained from the exact solution of the linearized problem as $J \to \infty$ ($\nu \to 0$, say) for both the drop and the bubble.

5 Exact solution of the linearized fully viscous problem

In this section we review the analysis of the effect of viscosity on small oscillations of a drop immersed in a vacuum and a bubble of negligible density and viscosity embedded in a viscous liquid by solving the linearized equations of motion without the assumption of irrotational flow. The procedure utilized by Reid (1960) for the case of the drop is summarized. The solution for the bubble is obtained following a similar path. In both cases, the dispersion relation shall coincide with the corresponding limiting results presented by Miller and Scriven (1968) and Prosperetti (1980a), who posed and solved the most general two-fluid problem.

5.1 Spherical drop

The linearized equation of motion for a liquid drop in $0 \leq r < a$ in the disturbed state is given by

$$\rho\frac{\partial \boldsymbol{u}}{\partial t} = -\nabla p + \mu\nabla^2\boldsymbol{u}, \tag{5.1}$$

with $\nabla \cdot \boldsymbol{u} = 0$.

Taking the divergence of (5.1), we have the equation for p

$$\nabla^2 p = 0 \tag{5.2}$$

for which we may express the pressure disturbance as

$$p = \rho A\,(r/a)^\ell\, Y_\ell^m(\theta,\varphi)\epsilon = \rho A x^\ell Y_\ell^m(\theta,\varphi)\epsilon, \tag{5.3}$$

with $\epsilon = \epsilon_0 \mathrm{e}^{-\sigma t}$ and $x = r/a$. For the disturbance of the spherical shape ζ, using normal modes, we set

$$\zeta(\theta,\varphi) = a\epsilon Y_\ell^m(\theta,\varphi), \tag{5.4}$$

In particular, since ∇p is a solenoidal vector for which $\nabla \cdot \nabla p = \nabla^2 p = 0$, we may write,

$$\frac{1}{\rho}\nabla p \;=\; \nabla \times \nabla \times \left[P(r)Y_\ell^m(\theta,\varphi)\epsilon \boldsymbol{e}_r\right], \tag{5.5}$$

such that the radial component is

$$\frac{1}{\rho}\left(\nabla p\right)_r \;=\; P(r)\epsilon\frac{\ell\,(\ell+1)}{r^2}Y_\ell^m = \epsilon\sigma^2 r\frac{\Pi(x)}{x^2}Y_\ell^m = A\frac{\ell}{r}x^{\ell-1}Y_\ell^m\epsilon, \tag{5.6}$$

which gives rise to the following relation,

$$\Pi(x) = \frac{A\ell}{\sigma^2 r^2}x^{\ell+1} = \Pi_0 x^{\ell+1}, \quad \Pi_0 = \frac{A\ell}{\sigma^2 r^2}, \tag{5.7}$$

with ∇p being a purely poloidal vector field. Since the velocity field $\boldsymbol{u}$ is solenoidal and ∇p is purely poloidal, it follows that $\boldsymbol{u}$ must be also purely poloidal (Reid, 1960). Thus, $\boldsymbol{u}$ can be expressed in terms of a single scalar function. By doing so, the radial component of the velocity may be written as

$$u_r = U(r)\epsilon\frac{\ell\left(\ell+1\right)}{r^2}Y_\ell^m = \epsilon\frac{\sigma r}{x^2}U(x)Y_\ell^m, \tag{5.8}$$

and for $\boldsymbol{r}\cdot\boldsymbol{u} = ru_r$, we have

$$\left(\frac{\partial}{\partial t} - \nu\nabla^2\right)\boldsymbol{r}\cdot\boldsymbol{u} = -\frac{1}{\rho}\boldsymbol{r}\cdot\nabla p, \tag{5.9}$$

Using (5.6) and (5.8) in (5.9), a differential equation for $U(x)$ can be written

$$\frac{\mathrm{d}^2U}{\mathrm{d}x^2} + \left[q^2 - \frac{\ell\left(\ell+1\right)}{x^2}\right]U = q^2\Pi(x), \tag{5.10}$$

with $q^2 = \frac{\sigma}{\nu}a^2$. The solution is

$$U(x) = C_1\sqrt{qx}J_{\ell+1/2}(qx) + \Pi(x) = U_1(x) + \Pi_0 x^{\ell+1} \tag{5.11}$$

The linearized kinematic condition at $x = 1$ is given in (2.19). Using (5.4), (5.8) and (5.11), this condition yields

$$C_1\sqrt{q}J_{\ell+1/2}(q) + \Pi_0 = -1. \tag{5.12}$$

The continuity of tangential and binormal stresses at the gas–liquid interface demands $\tau_{r\theta} = 0$ and $\tau_{r\varphi} = 0$ since the gas has negligible density and viscosity. The shear stresses can be computed from the velocity distribution in the drop. This condition at $x = 1$ leads to

$$C_1\left[\sqrt{q}\left[2\left(\ell^2-1\right) - q^2\right]J_{\ell+1/2}(q) + 2q\sqrt{q}J_{\ell+3/2}(q)\right] + 2\left(\ell^2-1\right)\Pi_0 = 0, \tag{5.13}$$

using expression (5.11) and a standard recursion relation for Bessel functions.

Expression (5.13) and the kinematic condition (5.12) give expressions for C_1 and Π_0

$$C_1 = -\frac{2\left(\ell^2-1\right)}{q^2\sqrt{q}J_{\ell+1/2}(q)}\Big/\left[1 - \frac{2}{q}Q^J_{\ell+1/2}\right], \tag{5.14}$$

$$\Pi_0 = -1 + \frac{2\left(\ell^2-1\right)}{q^2}\Big/\left[1 - \frac{2}{q}Q^J_{\ell+1/2}\right], \tag{5.15}$$

with

$$Q^J_{\ell+1/2}(q) = J_{\ell+3/2}(q)/J_{\ell+1/2}(q). \tag{5.16}$$

The normal stress balance at $x = 1$ for a drop surrounded by a gas of negligible density and viscosity can be derived from the more general expression in (2.18). Using (5.4), this condition becomes

$$p - 2\mu\frac{\partial u_r}{\partial r} = \frac{\gamma}{a^2}\left(\ell+2\right)\left(\ell-1\right)a\epsilon Y_\ell^m. \tag{5.17}$$

Applying previous results for p and u_r given in (5.3) and (5.8), we obtain

$$\Pi_0\sigma^2a^2 - 2\nu\sigma\ell\left[\frac{\mathrm{d}U}{\mathrm{d}x}\frac{1}{x^2} - \frac{2}{x^3}U\right]_{x=1} = \frac{\gamma}{\rho a}\ell\left(\ell+2\right)\left(\ell-1\right). \tag{5.18}$$

Setting the parameters

$$\alpha^2 = \frac{\sigma_D^* a^2}{\nu} = \hat{\sigma}_D^* \sqrt{J}, \qquad \frac{q^2}{\alpha^2} = \frac{\sigma}{\sigma_D^*} = \frac{\hat{\sigma}}{\hat{\sigma}_D^*}, \tag{5.19}$$

where σ_D^* is the frequency of oscillations from inviscid potential flow (IPF) given in (2.42). The normal stress balance is then arranged as

$$\Pi_0 q^4 - 2q^2 \ell \left[\left(\frac{\mathrm{d}U}{\mathrm{d}x} \right)_{x=1} + 2 \right] = \alpha^4 \tag{5.20}$$

From the solution for $U(x)$ in (5.11), one can compute dU/dx such that,

$$\left(\frac{\mathrm{d}U}{\mathrm{d}x} \right)_{x=1} + 2 = -(\ell - 1) + \left(\ell^2 - 1 \right) \frac{2}{q} Q^J_{\ell+1/2} \Big/ \left[1 - \frac{2}{q} Q^J_{\ell+1/2} \right], \tag{5.21}$$

where we have used the expressions for C_1 and Π_0 from (5.14) and (5.15).

Finally, replacing (5.15) and (5.21) into (5.20), the dispersion relation for the eigenvalue σ is obtained

$$\alpha^4 = 2q^2 (\ell - 1) \left[\ell + (\ell + 1) \frac{q - 2\ell Q^J_{\ell+1/2}}{q - 2Q^J_{\ell+1/2}} \right] - q^4 \tag{5.22}$$

A through discussion on the solution of (5.22) is presented by Chandrasekhar (1959, 1961) when q is real. Considering ℓ fixed, the R.H.S. of (5.22) is a function of q, $\Phi(q)$ say. The graph of this function on the axis of positive q reveals that there is an infinite number of intervals where $\Phi(q)$ is positive. The first of these intervals, which contains $q = 0$, encloses a maximum ($\alpha^2_{\max}$). For $\alpha^2 < \alpha^2_{\max}$ this first interval gives two real roots of (5.22), which determine the slowest rates of decay. Since $\alpha^2 = \hat{\sigma}_D \sqrt{J}$, for every mode ℓ, the magnitude of the Reynolds number J defines the roots. In the other intervals, one has $0 \leq \Phi(q) < \infty$. When $\alpha^2 > \alpha^2_{\max}$, (5.22) admits complex-conjugate eigenvalues with positive real parts which give the lowest rate of decay; these waves oscillate as they decay. Results from this dispersion relation are presented and discussed in §8.

As $J \to 0$, the rate of decay from the exact solution of a drop surrounded by gas behaves as

$$\hat{\sigma} = \hat{\sigma}_D^{*2} \sqrt{J} \frac{2\ell + 1}{2(\ell - 1)(2\ell^2 + 4\ell + 3)} \qquad \text{or} \qquad \sigma = \sigma_D^{*2} \frac{a^2}{\nu} \frac{2\ell + 1}{2(\ell - 1)(2\ell^2 + 4\ell + 3)}. \tag{5.23}$$

From the exact solution given above the behavior of the complex eigenvalue σ for the drop as $J \to \infty$ is

$$\hat{\sigma} = \frac{(2\ell + 1)(\ell - 1)}{\sqrt{J}} \pm i\hat{\sigma}_D^* \qquad \text{or} \qquad \sigma = \frac{\nu}{a^2}(2\ell + 1)(\ell - 1) \pm i\sigma_D^*. \tag{5.24}$$

These expressions were also obtained by Chandrasekhar (1959, 1961) and Miller & Scriven (1968). The result given in (3.24) from VCVPF is the same as the expression obtained in (5.24) from the exact solution.

5.2 Spherical bubble

To determine the eigenvalue relation for a bubble using normal modes, we follow closely the procedure described for a drop. The equation of motion for a liquid outside a bubble with small disturbances

at the interface $r = a$ is again (5.1) in the infinite region $a < r < \infty$. The pressure disturbance is harmonic and may be expressed as

$$p = \rho B \left(r/a\right)^{-\ell-1} Y_\ell^m(\theta,\varphi)\epsilon = \rho B x^{-\ell-1} Y_\ell^m(\theta,\varphi)\epsilon \tag{5.25}$$

for the liquid domain. The radial component of ∇p can be written as

$$\frac{1}{\rho}\left(\nabla p\right)_r \;=\; P(r)\epsilon\frac{\ell\left(\ell+1\right)}{r^2}Y_\ell^m = \epsilon\sigma^2 a\frac{\Pi(x)}{x^2}Y_\ell^m = -\left(\ell+1\right)B\frac{x^{-\ell-2}}{a}Y_\ell^m\epsilon, \tag{5.26}$$

giving rise to

$$\Pi(x) = -\frac{B\left(\ell+1\right)}{\sigma^2 a^2}x^{-\ell} = \Pi_0 x^{-\ell}, \quad \Pi_0 = -\frac{B\left(\ell+1\right)}{\sigma^2 a^2}. \tag{5.27}$$

The radial component of the velocity is

$$u_r \;=\; U(r)\epsilon\frac{\ell\left(\ell+1\right)}{r^2}Y_\ell^m = \epsilon\frac{\sigma a}{x^2}U(x)Y_\ell^m. \tag{5.28}$$

A differential equation can be obtained for $U(x)$ which is exactly as (5.10) with solution

$$U(x) = C_2\sqrt{qx}H_{\ell+1/2}^{(1)}(qx) + \Pi(x) = U_2(x) + \Pi_0 x^{-\ell}, \tag{5.29}$$

where $H_{\ell+1/2}^{(1)}$ is the Hankel function of the first kind of half integer order and we choose $\mathrm{Im}(\sigma) > 0$. The kinematic condition at $x = 1$ yields

$$C_2\sqrt{q}H_{\ell+1/2}^{(1)}(q) + \Pi_0 = -1. \tag{5.30}$$

The continuity of tangential and binormal stresses at $x = 1$ leads to

$$C_2\left[\sqrt{q}\left[2\left(\ell^2-1\right)-q^2\right]H_{\ell+1/2}^{(1)}(q) + 2q\sqrt{q}H_{\ell+3/2}^{(1)}(q)\right] + 2\ell\left(\ell+2\right)\Pi_0 = 0. \tag{5.31}$$

Expressions (5.30) and (5.31) give C_2 and Π_0. The normal stress balance at $x = 1$ obtained from (2.18) when the density and viscosity of the inner fluid are put to zero yields

$$\Pi_0 q^4 + 2q^2\left(\ell+1\right)\left[\left(\frac{\mathrm{d}U}{\mathrm{d}x}\right)_{x=1} + 2\right] = \alpha^4 \tag{5.32}$$

using the relations (5.19). In these relations, the eigenvalue σ_B given in (4.28) for a bubble is used instead of σ_D. From the solution $U(x)$ in (5.29) an expression for $\mathrm{d}U/\mathrm{d}x$ can be computed and evaluated at $x = 1$. Substitution of this result and the expression for Π_0 in the normal stress balance (5.32) leads to the dispersion relation for the eigenvalue σ in the case of the bubble,

$$\alpha^4 = \left(\ell+2\right)q^2\frac{\left(2\ell+1\right)q^2 - 2\left(\ell+1\right)\left(\ell-1\right)\left[\left(2\ell+1\right) - qQ_{\ell+1/2}^H\right]}{\left(2\ell+1\right) + q^2/2 - qQ_{\ell+1/2}^H} - q^4, \tag{5.33}$$

with

$$Q_{\ell+1/2}^H = H_{\ell+3/2}^{(1)}(q)/H_{\ell+1/2}^{(1)}(q). \tag{5.34}$$

The same dispersion relation found by Miller & Scriven (1968). Prosperetti (1980a) indicates that this dispersion relation only admits complex roots as a consequence of the character of the Hankel funtions. Therefore, for a bubble, only progressive–decaying waves are predicted. For a drop, we recall that real eigenvalues can be found. On physical grounds, Prosperetti (1980a) argues that the complex nature of the eigenvalues for a bubble is related to the unboundedness of the fluid domain – in contrast with the finite amount of fluid require for a drop–, since an infinite domain provides an efficient mechanism for smoothing out the velocity gradients. Another feature of the dispersion relation is that the solutions occur in conjugate pairs, as in the drop case, since, for $\mathrm{Im}(\sigma) < 0$, one can choose the Hankel function of the second kind in (5.29), and (5.33) is satisfied.

For a gas bubble in a viscous liquid, a real σ can be approximated as $J \to 0$,

$$\hat{\sigma} = \hat{\sigma}_B^{*2}\sqrt{J}\frac{2\ell+1}{2(2\ell^2+1)(\ell+2)} \qquad \text{or} \qquad \sigma = \sigma_B^{*2}\frac{a^2}{\nu}\frac{2\ell+1}{2(2\ell^2+1)(\ell+2)}, \tag{5.35}$$

For $J \to \infty$, damped-progressive waves take place with eigenvalues

$$\hat{\sigma} = \frac{(2\ell+1)(\ell+2)}{\sqrt{J}} \pm i\hat{\sigma}_B^* \qquad \text{or} \qquad \sigma = \frac{\nu}{a^2}(2\ell+1)(\ell+2) \pm i\sigma_B^*. \tag{5.36}$$

Both results presented by Miller & Scriven (1968). As in the case of the drop, the result obtained from VCVPF in (4.35) is the same as the expression given in (5.36) from the exact solution.

6 Dissipation approximation

Viscous effects can be included for irrotational motion through the dissipation method; neither vortical layers nor viscous corrections enter into the analysis. This method stems from the evaluation of the mechanical energy equation on the fluid domain. In this equation, the viscous dissipation in the bulk of the liquid is approximated by potential flow, while the continuity of tangential stress is enforced at the gas-liquid interface; the shear stress is put to zero (the gas being considered of negligible density and viscosity). Lamb (1932) found the exact solution for the decay rate of free gravity waves in complete agreement with the decay rate from the dissipation method. Lamb (1881, 1932) also used the dissipation method to compute the decay rate for small progressive waves in the free surface of a liquid spherical drop immersed in gas and a spherical bubble surrounded by liquid. For several problems involving free surfaces, Joseph & Wang (2004) showed that the dissipation method and VCVPF give the same result. This set of problems includes the drag force on a spherical or oblate ellipsoidal gas bubble and the decay rate of free gravity waves. The same conclusion was reached by Wang *et al.* (2005a, 2005b) for the decay rate of capillary instability. Here, the procedure described in their work is applied to the spherical geometry. We show that the dissipation method gives rise to the same dispersion relation as VCVPF. Our result goes further than Lamb's, since the effect of viscosity in the frequency of the oscillations is predicted in the analysis that follows.

In the case of a liquid drop surrounded by a vacuum, the mechanical energy equation can be written as

$$\frac{d}{dt}\int_V \rho\frac{|\boldsymbol{u}|^2}{2}\mathrm{d}V = \int_A \boldsymbol{n}\cdot\boldsymbol{T}\cdot\boldsymbol{u}\mathrm{d}A - \int_V 2\mu\boldsymbol{D}:\boldsymbol{D}\mathrm{d}V, \tag{6.1}$$

where, $\boldsymbol{T}$ is taken as the stress tensor for Newtonian incompressible flow and $\boldsymbol{D}$ is the strain rate tensor. The last term in (6.1) represents the viscous dissipation. For potential flow, the following identity holds,

$$\int_V 2\mu \boldsymbol{D} : \boldsymbol{D} \mathrm{d}V = \int_A \boldsymbol{n} \cdot 2\mu \boldsymbol{D} \cdot \boldsymbol{u} \mathrm{d}A. \tag{6.2}$$

Therefore, (6.1) becomes,

$$\frac{d}{dt}\int_V \rho \frac{|\boldsymbol{u}|^2}{2} \mathrm{d}V = \int_A [(-p + \tau_{rr})u_r + \tau_{r\theta} u_\theta + \tau_{r\varphi} u_\varphi] \mathrm{d}A - \int_A \boldsymbol{n} \cdot 2\mu \boldsymbol{D} \cdot \boldsymbol{u} \mathrm{d}A. \tag{6.3}$$

At the free surface $r = a$, we recall that the normal stress balance gives rise to,

$$-p + \tau_{rr} = -\frac{\gamma}{a^2}(L^2 - 2)\zeta. \tag{6.4}$$

The shear stresses are zero at the free surface

$$\tau_{r\theta} = 0, \qquad \tau_{r\varphi} = 0. \tag{6.5}$$

With these boundary conditions, the mechanical energy equation (6.3) can be expressed as

$$\frac{d}{dt}\int_V \rho \frac{|\boldsymbol{u}|^2}{2} \mathrm{d}V = -\int_A \frac{\gamma}{a^2}(L^2 - 2)\zeta u_r \mathrm{d}A - \int_A \boldsymbol{n} \cdot 2\mu \boldsymbol{D} \cdot \boldsymbol{u} \mathrm{d}A. \tag{6.6}$$

With $|\boldsymbol{u}|^2 = u_r^2 + u_\theta^2 + u_\varphi^2$ and the components of $\boldsymbol{D}$ expressed in spherical coordinates, the integrals in (6.6) can be evaluated (see Appendix)

$$\begin{aligned} \frac{d}{dt}\int_V \rho \frac{|\boldsymbol{u}|^2}{2} \mathrm{d}V &= \sum_{\ell=0}^{\infty}\sum_{m=0}^{\ell} F_{\ell m} 4\pi a \rho \left(A_\ell e^{-\sigma_\ell t} + \bar{A}_\ell e^{-\bar{\sigma}_\ell t}\right) \\ &\quad \left(-\sigma_\ell A_\ell e^{-\sigma_\ell t} - \bar{\sigma}_\ell \bar{A}_\ell e^{-\bar{\sigma}_\ell t}\right) \frac{\ell}{2\ell+1}\frac{(\ell+m)!}{(\ell-m)!}, \end{aligned} \tag{6.7}$$

$$\begin{aligned} \int_A \frac{\gamma}{a^2}(L^2 - 2)\zeta u_r \mathrm{d}A &= \sum_{\ell=0}^{\infty}\sum_{m=0}^{\ell} F_{\ell m} 4\pi \frac{\gamma}{a^2} \left(A_\ell e^{-\sigma_\ell t} + \bar{A}_\ell e^{-\bar{\sigma}_\ell t}\right) \\ &\quad \left(-\frac{A_\ell}{\sigma_\ell} e^{-\sigma_\ell t} - \frac{\bar{A}_\ell}{\bar{\sigma}_\ell} e^{-\bar{\sigma}_\ell t}\right) \frac{(\ell+2)\ell^2(\ell-1)}{2\ell+1}\frac{(\ell+m)!}{(\ell-m)!}, \end{aligned} \tag{6.8}$$

and

$$\int_A \boldsymbol{n} \cdot 2\mu \boldsymbol{D} \cdot \boldsymbol{u} \mathrm{d}A = \sum_{\ell=0}^{\infty}\sum_{m=0}^{\ell} F_{\ell m} \frac{8\pi\mu}{a} \left(A_\ell e^{-\sigma_\ell t} + \bar{A}_\ell e^{-\bar{\sigma}_\ell t}\right)^2 \ell(\ell-1)\frac{(\ell+m)!}{(\ell-m)!}. \tag{6.9}$$

Substitution into (6.6) yields (dropping the subscript ℓ),

$$\begin{aligned} -\left(\sigma A e^{-\sigma t} + \bar{\sigma}\bar{A} e^{-\bar{\sigma} t}\right) &= \frac{\gamma}{\rho a^3}\left(\frac{A}{\sigma} e^{-\sigma t} + \frac{\bar{A}}{\bar{\sigma}} e^{-\bar{\sigma} t}\right)(\ell+2)\ell(\ell-1) \\ &\quad -\frac{2\nu}{a^2}\left(A e^{-\sigma t} + \bar{A} e^{-\bar{\sigma} t}\right)(2\ell+1)(\ell-1), \end{aligned} \tag{6.10}$$

which has the form,

$$\left[-\sigma + \frac{2\nu}{a^2}(2\ell+1)(\ell-1) - \frac{\gamma}{\rho a^3 \sigma}(\ell+2)\ell(\ell-1)\right] A e^{-\sigma t} + \text{c.c.} = 0. \tag{6.11}$$

Therefore, the same dispersion relation (3.20) obtained from VCVPF is recovered from the dissipation approximation

$$\sigma^2 - \frac{2\nu}{a^2}(2\ell+1)(\ell-1)\sigma + \frac{\gamma}{\rho a^3}(\ell+2)\ell(\ell-1) = 0. \tag{6.12}$$

Following the same steps, the dispersion relation (4.29) from VCVPF can also be obtained from the dissipation method for the case of a spherical bubble immersed in liquid.

7 VPF and VCVPF analyses for waves acting on a plane interface considering surface tension – Comparison with Lamb's solution

The problem of the viscous effects on free gravity waves was solved exactly by Lamb (1932). In his analysis, surface tension effects were included. Joseph & Wang (2004) gave a solution to this problem using viscous potential flow (VPF). They also added a viscous correction to the irrotational pressure and obtained another dispersion relation for the complex eigenvalue σ. In their analysis they neglected the surface tension effects and considered gravity effects. Here we find the rate of decay and wave velocity for free waves on an otherwise plane interface neglecting gravity effects and including surface tension. These expressions are found as limiting results from our VPF and VCVPF analyses of waves on the surface of a liquid drop surrounded by gas. This procedure considers taking the limits $\ell \to \infty$ and $a \to \infty$ such that $\ell/a \to k$ in the expressions for the complex eigenvalue σ (Miller& Scriven 1968).

For VPF, in the case of $k > k_c = \gamma/\rho\nu^2$, the decay rate is

$$\sigma = \nu k^2 \pm \sqrt{(\nu k^2)^2 - \gamma k^3/\rho}. \tag{7.1}$$

If $k < k_c = \gamma/\rho\nu^2$ then we have

$$\sigma = \nu k^2 \pm ik\sqrt{\gamma k/\rho - \nu^2 k^2}, \tag{7.2}$$

such that the wave-velocity is $c = \sqrt{\gamma k/\rho - \nu^2 k^2}$ and the rate of decay is νk^2.

Studying the asymptotic behavior for $k >> k_c = \gamma/\rho\nu^2$, the rate of decay goes as

$$\sigma_1 = \frac{\gamma k}{2\rho\nu}, \tag{7.3}$$

$$\sigma_2 = 2\nu k^2. \tag{7.4}$$

Then, σ_1 gives the slowest rate of decay for large k.

On the other hand, the asymptotic behavior as $k << k_c = \gamma/\rho\nu^2$ can be expressed as

$$\sigma = \nu k^2 \pm ik\sqrt{\gamma k/\rho}, \tag{7.5}$$

such that the wave velocity is given by $c = \sqrt{\gamma k/\rho}$; this is the same result from IPF as shown below. The rate of decay goes as νk^2.

For VCVPF, in the case of $k > k_c = \gamma/4\rho\nu^2$, the rate of decay is

$$\sigma = 2\nu k^2 \pm \sqrt{(2\nu k^2)^2 - \gamma k^3/\rho}. \tag{7.6}$$

If $k < k_c = \gamma/4\rho\nu^2$ then we have

$$\sigma = 2\nu k^2 \pm ik\sqrt{\gamma k/\rho - 4\nu^2 k^2}, \tag{7.7}$$

such that the wave-velocity is $c = \sqrt{\gamma k/\rho - 4\nu^2 k^2}$ and the rate of decay is $2\nu k^2$.

Studying the asymptotic behavior for $k >> k_c = \gamma/4\rho\nu^2$ the rate of decay goes as

$$\sigma_1 = \frac{\gamma k}{4\rho\nu}, \tag{7.8}$$

and

$$\sigma_2 = 4\nu k^2, \tag{7.9}$$

and σ_1 gives the slowest rate of decay for large k.

On the other hand, the asymptotic behavior as $k << k_c = \gamma/4\rho\nu^2$ can be expressed as

$$\sigma = 2\nu k^2 \pm ik\sqrt{\gamma k/\rho}, \tag{7.10}$$

such that the wave velocity is given by $c = \sqrt{\gamma k/\rho}$, which is the same result from inviscid potential flow (IPF) as shown below. In this case the rate of decay goes as $2\nu k^2$. It can be verified that the same results are found if one starts from the VPF and VCVPF solutions obtained for a bubble surrounded by a viscous liquid.

Lamb (1932) solved the problem of free gravity waves exactly considering the effects of surface tension (art. 349, pp. 625). Lamb's dispersion relation, neglecting gravitational effects, is

$$(\sigma - 2\nu k^2)^2 + \frac{\gamma}{\rho}k^3 = 4\nu^2 k^3 m, \tag{7.11}$$

with

$$m^2 = k^2 - \sigma/\nu.$$

Therefore, the dispersion relation is biquadratic. As the viscosity goes to zero, Lamb found that the complex eigenvalue σ behaves as

$$\sigma = 2\nu k^2 \pm ik\sqrt{\gamma k/\rho}, \tag{7.12}$$

which is exactly the result from VCVPF in the case of $k << k_c = \gamma/4\rho\nu^2$. In the limit $\nu \to 0$ Lamb's exact solution reduces to

$$\sigma_P^2 = \gamma k^3/\rho, \tag{7.13}$$

corresponding to IPF analysis. Then, the wave-velocity for inviscid flow is $c = \sqrt{\gamma k/\rho}$, as mentioned above.

For the case of $\nu \to \infty$, Lamb (1932) found two real roots from his exact solution neglecting surface tension. Following the same procedure but neglecting gravity effects and keeping surface tension, we find that the relevant root on physical grounds is

$$\sigma = \frac{\gamma k}{2\rho\nu}, \tag{7.14}$$

which is the same result obtained from VPF in (7.3). Using asymptotic formulas for Bessel functions of large order and large variable such that $a \to \infty$ and $\ell \to \infty$ for fixed k, Prosperetti (1980a) showed that the dispersion relation for the bubble (5.33) reduces to Lamb's result (7.11). Prosperetti (1976) posed and solved the initial value problem for small disturbances of the infinite plane without assuming an exponential decay with time. For an irrotational initial condition and neglecting gravity, in the limit $t \to 0$, his dispersion relation is the same as (7.7), obtained here by a different method.

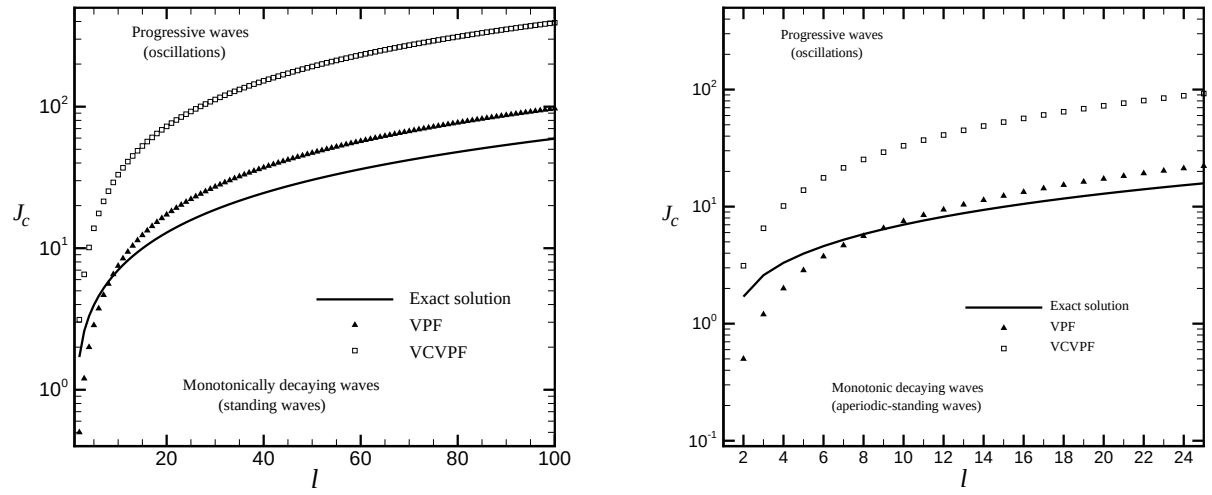

(a) wide spectrum (b) zoomed view

Figure 1: Critical Reynolds number J_c as a function of the mode number ℓ for a *drop*. At a given ℓ, for $J > J_c$ progressive decaying waves (oscillations) are predicted (i.e. the eigenvalues $\hat{\sigma}$ are complex), whereas for $J \leq J_c$ monotonically decaying waves are obtained (i.e. the eigenvalues $\hat{\sigma}$ are real): (a) for $2 \leq l \leq 100$ and (b) zoom for $2 \leq l \leq 25$. The results are presented for VPF, VCVPF and the exact solution.

8 Results and Discussion

In this section, a detailed comparison of the results for the decay rate and frequency of the waves according to VPF and VCVPF with the exact solutions of the fully viscous linear problem are presented for a drop and a bubble. A wide interval is selected for the mode number ℓ ranging from $\ell = 2$ up to $\ell = 100$. The smallest value of $\ell = 2$ is chosen since lower values yield compressive or expansive motions of the drop interface which are not compatible with the incompressibility assumption or a non-physical static disturbed interface. For higher values of ℓ the exact fully viscous solution for the drop predicts oscillations that decay faster (Miller & Scriven, 1968). The same lowest value of $\ell = 2$ is selected for the bubble case.

Figure 1 shows the critical Reynolds number J_c as a function of ℓ for a drop. The critical Reynolds number is defined as the value of J at a given ℓ for which transition from monotonically decaying waves to progressive waves (oscillations) occurs. For $J \leq J_c$ the eigenvalues $\hat{\sigma}$ are real and monotonically decaying waves take place, whereas for $J > J_c$ the eigenvalues are complex and the waves decay through oscillations. Notice that when $J > J_c$ from VCVPF all the three theories predicts progressive waves. On the other hand, for $J < J_c$ from the exact solution all the theories predict monotonically decaying waves except for the lower interval $\ell \leq 8$ where VPF gives rise to lower values of J_c. In between, at least one approach (VCVPF) will predict standing waves. For $\ell > 8$, VPF predicts a J_c value bounded by the critical values resulting from the other two theories. Figure 2 presents the trends of J_c with ℓ for VPF and VCVPF for a bubble. Recall that the exact solution always predicts decaying oscillations (i.e. complex eigenvalues) in the bubble case. Therefore, the exact solution does not give rise to a critical J. If VCVPF predicts progressive decaying waves, then VPF gives the same prediction. If VPF predicts standing waves, then the same behavior is obtained from VCVPF.

For a drop, the decay rate and wave frequency as a function of the Reynolds number J are presented

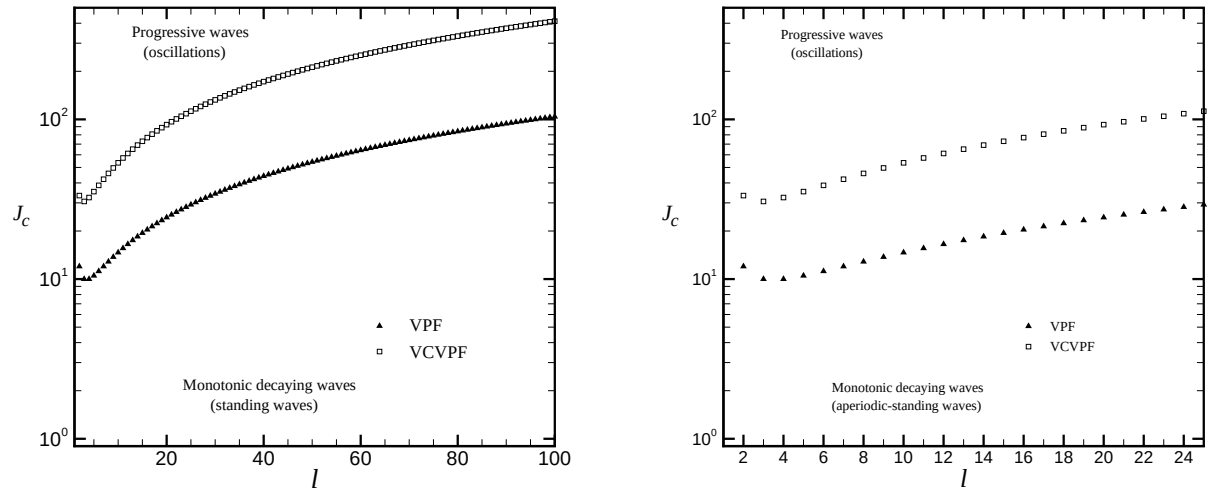

(a) wide spectrum (b) zoomed view

Figure 2: Critical Reynolds number J_c as a function of the mode number ℓ for a *bubble*. At a given ℓ, for $J > J_c$ progressive decaying waves (oscillations) are predicted (i.e. the eigenvalues $\hat{\sigma}$ are complex), whereas for $J \leq J_c$ monotonically decaying waves are obtained (i.e. the eigenvalues $\hat{\sigma}$ are real): (a) for $2 \leq l \leq 100$ and (b) zoom for $2 \leq l \leq 25$. The results are presented for VPF and VCVPF. Notice that the exact solution given by the fully viscous flow approach does not provide a crossover value, since the imaginary part is never identically zero.

in Figure 3 (a) and (b), respectively, for $\ell = 2$ as predicted by VPF, VCVPF and the exact solution. The wave frequency given by IPF is also included for comparison. Recall that IPF yields zero decay rate. For large J, VCVPF and the exact solution show excellent agreement, whereas VPF is off the mark by -60%. The wave frequencies from the three viscous theories tend to the inviscid solution for large J. As J decreases (below $J = 10$, say), transition from the progressive waves regime to the standing waves regime occurs. In the point of transition, the frequency becomes identically zero, the eigenvalue $\hat{\sigma}$ becomes purely real and the curve of $\mathrm{Re}(\hat{\sigma})$ bifurcates yielding two real and different roots. In Figure 3 (a), the lowest root, representing the least damped mode of decay, is presented. With decreasing J, from the asymptotic behavior of the different theories, one can readily find that VPF and VCVPF show a relative discrepancy of 90% and -24%, respectively, with respect to the exact solution for $\ell = 2$.

For a bubble, the rate of decay is presented in Figure 4 (a) whereas the wave frequency is shown in Figure 4 (b). Notice that the results follow similar trends as those described above for the drop. An important difference, however, is that the exact solution does not predict transition to the standing waves regime, but the wave frequency tends smoothly to zero as J decreases (the viscosity increases, say). Thus, no critical cross-over value J_c exists according to the exact theory and the oscillations are never completely damped, though the frequency can reach very small magnitudes (see Figure 4 b). We do not have a satisfactory argument to explain, on physical grounds, this difference between the drop and the bubble on the response of the exact solution. On the other hand, the irrotational viscous theories, VPF and VCVPF do render a cross-over J_c for which transition to monotonically decaying waves occurs. Also notice that as $J \to 0$ the relative error with respect to the exact solution remains as -40% for VPF and -64% for VCVPF using the asymptotic expressions for $\ell = 2$. For large J, VPF

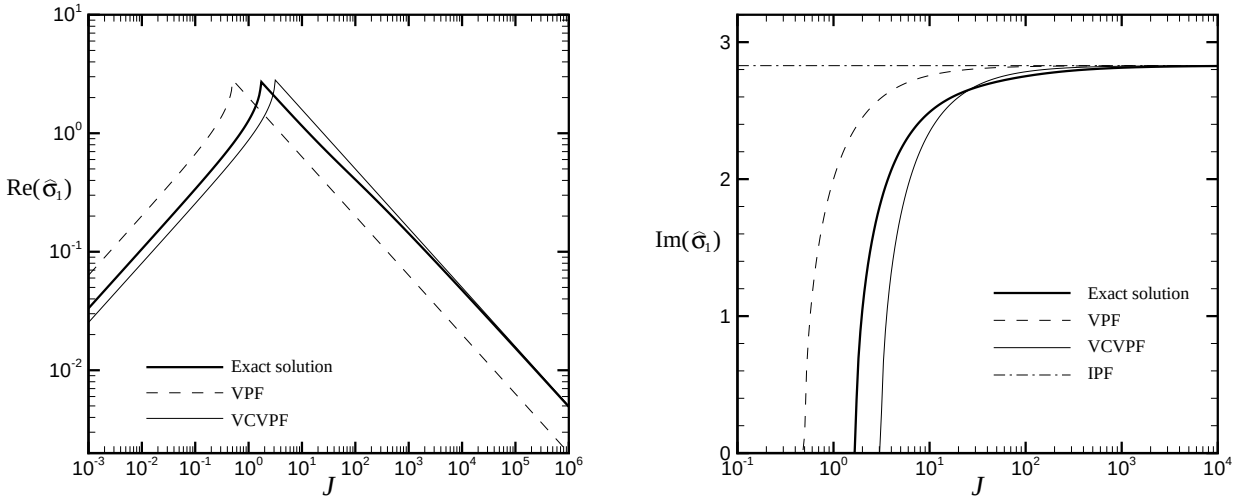

(a) Decay rate (b) Wave frequency

Figure 3: Decay rate and wave frequency for the fundamental mode $\ell = 2$ as function of the Reynolds number J for a *drop* from the exact solution, VPF, VCVPF and IPF. The decay rate predicted by IPF is identically zero for all ℓ.

is off the mark by -40% for the bubble.

For large values of J, if one of the fluids has negligible density and viscosity, a thin boundary layer results (Miller & Scriven 1968). Thus, an irrotational velocity field works as a good approximation with a pressure correction arising within the boundary layer and resolving the discrepancy between the non-zero irrotational shear stress and the actual zero shear stress at the interface. These considerations explain the excellent agreement of VCVPF and the exact solution for large J. In terms of the dissipation approximation, such a thin boundary layer yields a negligible contribution to the total viscous dissipation, which is thus determined by the irrotational flow. By contrast, as J decreases (e.g., the liquid viscosity increases), the boundary layer becomes thicker and the performance of the irrotational approximations (VPF and VCVPF) deteriorates. A non-negligible boundary layer flow contributes substantially to the rate of viscous dissipation. The motion for small J, as discussed by Prosperetti (1980a), is restrained in such a drastic way that the energy dissipation per unit time, and thus the decay rate, decrease with the Reynolds number J.

The sharp cross-over from the progressive waves regime to the standing waves regime can be readily obtained from the dispersion relations (Figure 3). For a bubble, oscillatory decaying waves are always predicted by the exact linearized theory yet the smooth region where the decay-rate graph reaches a maximum as a function of the Reynolds number J (Figure 4) suggests a transition in the structure of the flow. This was associated by Prosperetti (1980a) with the two length scales characteristic of the problem, namely, the sphere's radius a and the vorticity diffusion length of order $(\nu/\omega_B)^{1/2}$, where ω_B is the frequency of the oscillations for the inviscid case given in (4.28). For $a >> (\nu/\omega_B)^{1/2}$ a thin vorticity layer at the interface occurs, having a minute effect on the rate of viscous dissipation. In dimensionless form, this inequality can be written as

$$1 >> (\hat{\omega}_B \sqrt{J})^{-1/2}, \tag{8.1}$$

which represents the right branch of the exact solution in Figure 4 (a). As J increases, the frequency

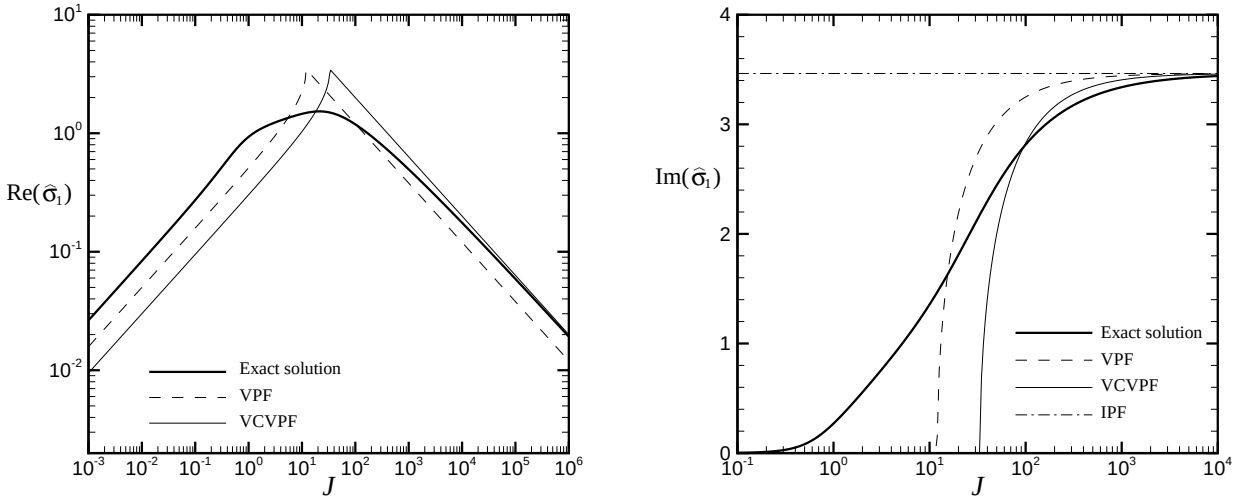

(a) Decay rate

(b) Wave frequency

Figure 4: Decay rate and wave frequency for the fundamental mode $\ell = 2$ as function of the Reynolds number J for a *bubble* from the exact solution, VPF, VCVPF and IPF. The decay rate predicted by IPF is identically zero for all ℓ.

of the oscillations approaches closely the inviscid frequency asymptote (see Figure 4 b). For an almost constant frequency, increasing J (i.e. decreasing ν, say) also reduces the rate of viscous dissipation and, as a consequence, the rate of decay of the oscillations. On the other hand, the left branch in Figure 4 (a), for which the rate of decay is reduced with decreasing J, as explained above, is associated with a relatively thicker vorticity layer such that $a << (\nu/\omega_B)^{1/2}$. In dimensionless form, this condition becomes,

$$1 << (\hat{\omega}_B \sqrt{J})^{-1/2}. \tag{8.2}$$

Figures 5 and 7 show results for the rate of decay of waves on the spherical interface for a drop and a bubble, respectively, from the three theories, VPF, VCVPF and the exact solution, for four mode numbers ($\ell = 2$, 3, 4 and 10). The features commented for the fundamental mode $\ell = 2$ are also observed for the other modes. Notice that as ℓ increases the rate of decay increases. Hence, the waves are more effectively damped for larger ℓ. From the approximate solutions VPF and VCVPF for the drop case, one can note that there is a very short interval of J at the cross-over peak (Figures 5 a and b) for which $\ell = 2$ has a decay rate larger than $\ell = 3$ and 4. A similar trend in a different J interval is observed for the pair of curves $\ell = 3$ and $\ell = 4$ on the same figures.

Figures 6 and 8 present the frequency of oscillations for the same four modes for a drop and a bubble, respectively. As J increases, the curves tend asymptotically to the inviscid frequency, which increases with ℓ. The analysis of the predictions from the exact solution indicates that the change-over from progressive waves to standing waves takes place for a larger critical J as ℓ increases for a drop (Figure 6 c). Even though no transition to standing waves occur, a somewhat similar behavior is observed for the bubble, since the frequency graph seems to lie close to the zero axis within a narrow tolerance for larger values of J as ℓ increases (Figure 8 c). These results for the drop and bubble show that viscosity damps the motion (either oscillatory or standing) more effectively for shorter waves, as expected.

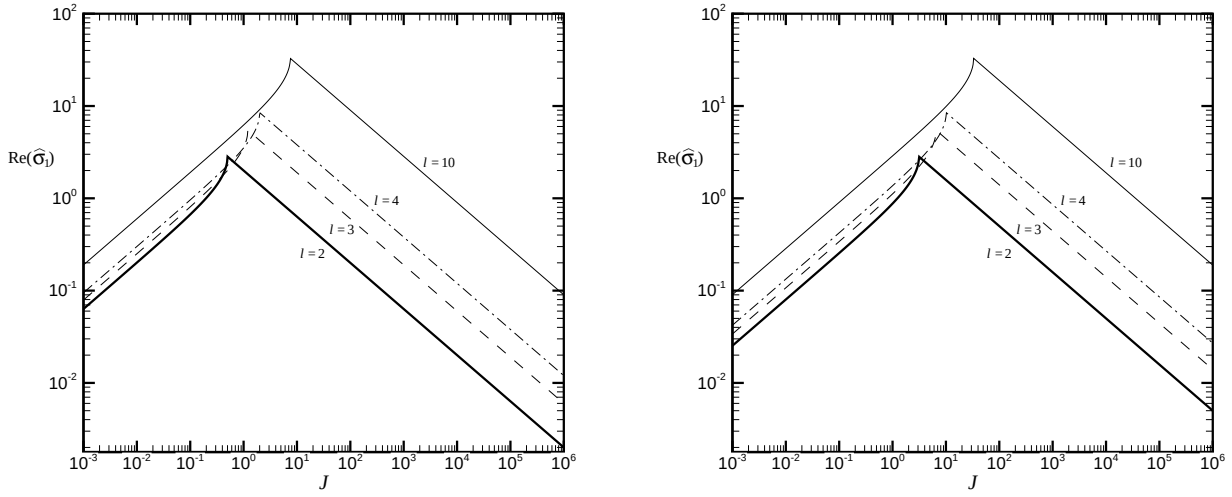

(a) VPF

(b) VCVPF

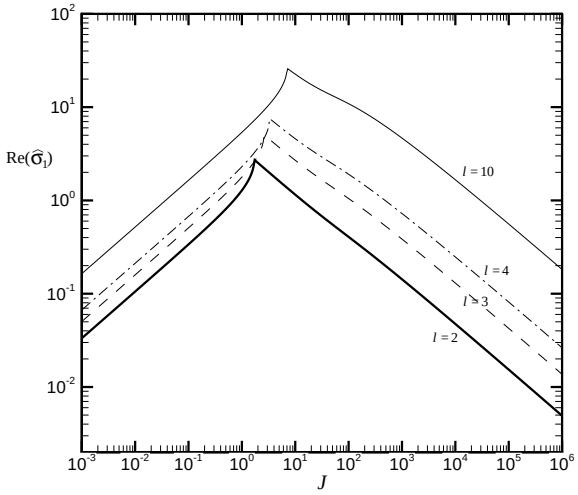

(c) Exact solution

Figure 5: Decay rate Re($\hat{\sigma}$) as a function of the Reynolds number J for four modes numbers $\ell = 2$, 3, 4 and 10, for a *drop*: (a) VPF, (b) VCVPF and (c) exact solution. The left branches of the curves that increase with J correspond to the lowest real eigenvalue $\hat{\sigma}_1$ (i.e. standing decaying waves). The branches of the curves that decrease with J refer to progressive decaying waves where the complex eigenvalues $\hat{\sigma}_1$ and $\hat{\sigma}_2$ are a conjugate pair. Recall that IPF predicts progressive waves with constant amplitude such that Re($\hat{\sigma}$)=0 for every ℓ.

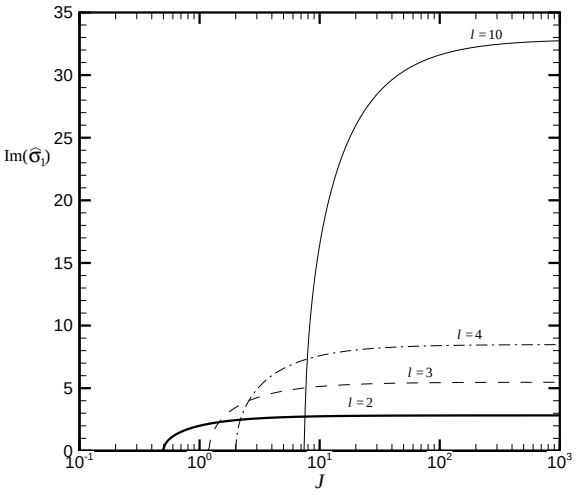

(a) VPF

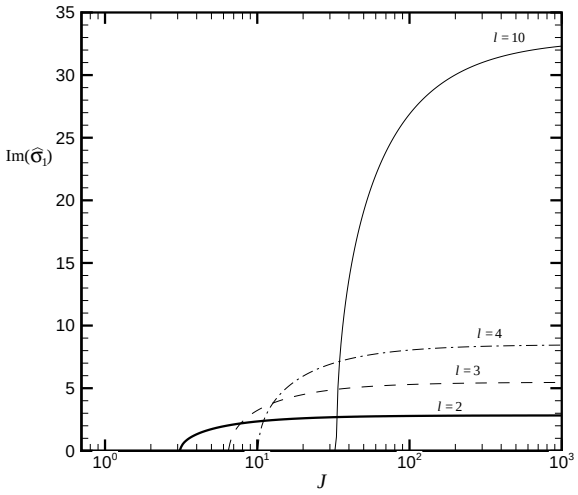

(b) VCVPF

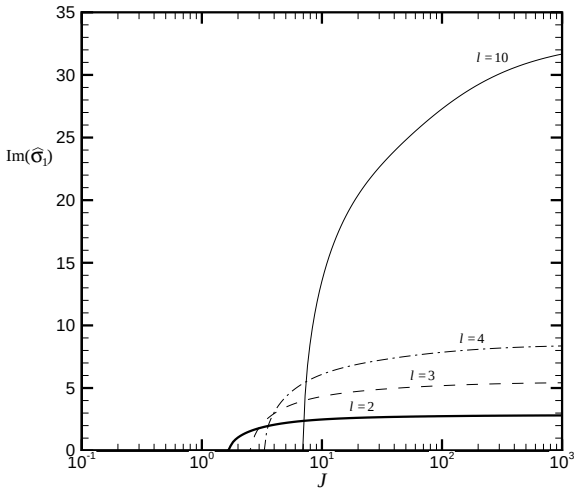

(c) Exact solution

Figure 6: Frequency $\mathrm{Im}(\hat{\sigma})$ as a function of the Reynolds number J for four modes numbers $\ell = 2$, 3, 4 and 10, for a *drop*: (a) VPF, (b) VCVPF and (c) exact solution. For every ℓ, there is a critical value of J for which $\mathrm{Im}(\hat{\sigma})$ vanishes. These critical values of J are presented in Figure 1 for VPF, VCVPF and the exact solution. For large J, the curves of $\mathrm{Im}(\hat{\sigma})$ approach IPF's solutions asymptotically in all the cases.

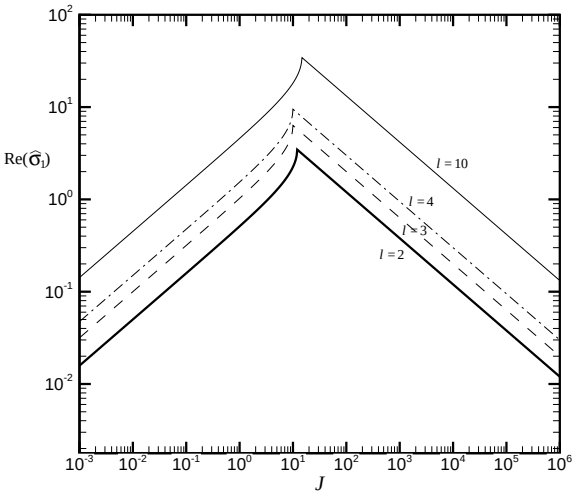

(a) VPF

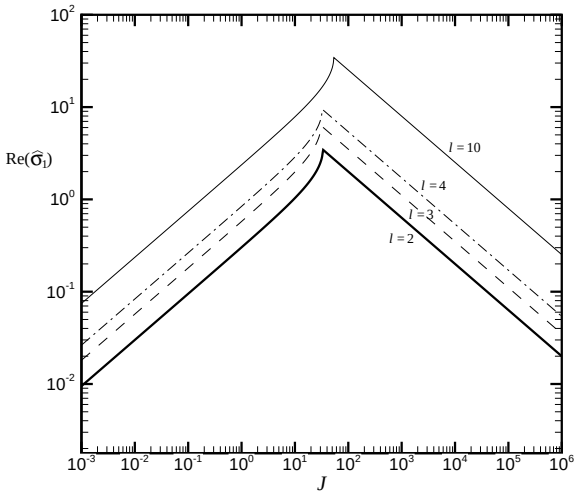

(b) VCVPF

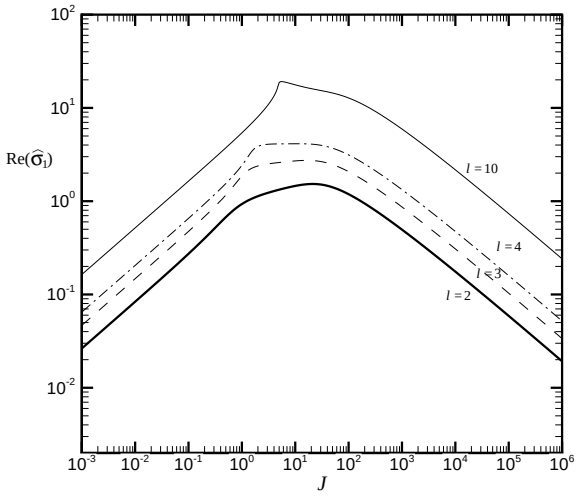

(c) Exact solution

Figure 7: Decay rate Re($\hat{\sigma}$) as a function of the Reynolds number J for four modes numbers ℓ = 2, 3, 4 and 10, for a *bubble*: (a) VPF, (b) VCVPF and (c) exact solution. For VPF and VCVPF, the left branches of the curves that increase with J correspond to the lowest real eigenvalue $\hat{\sigma}_1$ (i.e. standing decaying waves). The branches of the curves that decrease with J refer to progressive decaying waves where the complex eigenvalues $\hat{\sigma}_1$ and $\hat{\sigma}_2$ are a conjugate pair. According to the exact solution , the eigenvalues are complex with non–zero imaginary part (i.e. progressive decaying waves). Recall that IPF predicts progressive waves with constant amplitude such that Re($\hat{\sigma}$)=0 for every ℓ.

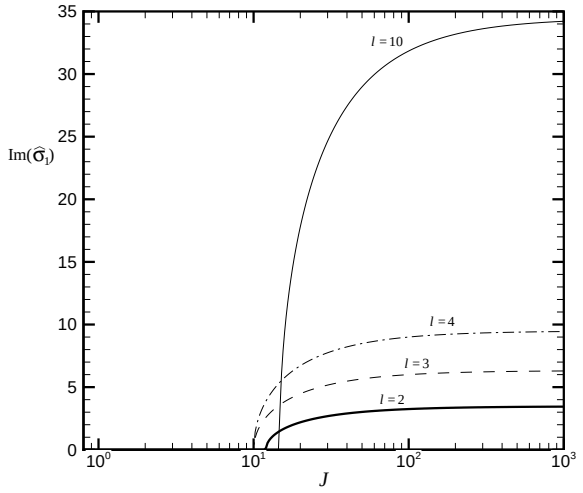

(a) VPF

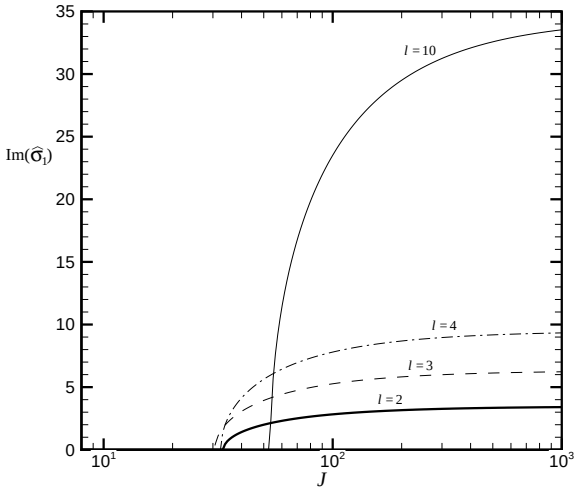

(b) VCVPF

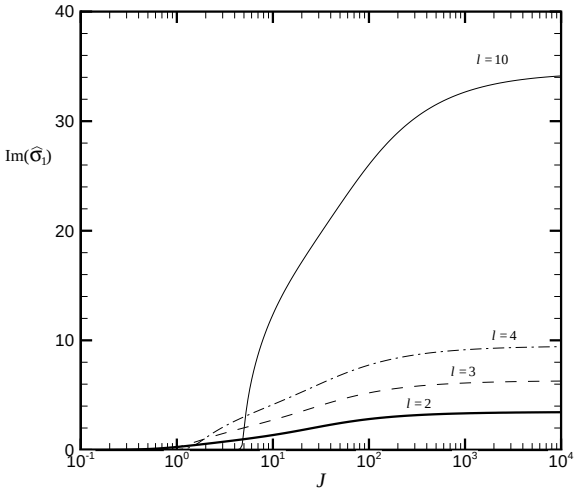

(c) Exact solution

Figure 8: Frequency $\mathrm{Im}(\hat{\sigma})$ as a function of the Reynolds number J for four modes numbers $\ell = 2$, 3, 4 and 10, for a *bubble*: (a) VPF, (b) VCVPF and (c) exact solution. For every ℓ, there is a critical value of J for which $\mathrm{Im}(\hat{\sigma})$ vanishes according to VPF and VCVPF approaches. These critical values of J are presented in Figure 2 for VPF, VCVPF. Notice that for the exact solution all the curves approach $\mathrm{Im}(\hat{\sigma}) = 0$ asymptotically through the smallest values of J. The imaginary part of the eigenvalue $\hat{\sigma}$ for the exact solution is only identically zero in the limit $J \to 0$. For large J, the curves of $\mathrm{Im}(\hat{\sigma})$ approach IPF's solutions asymptotically in all the cases.

For a drop, Figures 9 through 18 present predictions from VPF, VCVPF and the exact solution for the rate of decay and frequency of the oscillations for a bubble for several values of the Reynolds number J, namely, J =10^{-3}, 10, 40, 500 and 10^6. The results are presented as function of the mode number ℓ. The odd-numbered figures show the rate of decay, while the even-numbered figures show the frequency of the oscillations. For small J, in the standing waves regime, VCVPF gives a better approximation to the exact solution than VPF for the fundamental mode $\ell = 2$, as can be observed in Figure 9 for $J = 10^{-3}$. By contrast, for larger ℓ (i.e. shorter waves), VPF shows a better performance. Recall that the inviscid theory, IPF, gives zero decay rate for all ℓ. As J increases, the waves start to oscillate for low values of ℓ. For instance, in the case of $J = 10$, the cross-over values of ℓ according to every viscous theory enters the analysis (see Figure 11). In the cases considered in this study for which $J \geq 10$, the critical values of ℓ follows the trend $\ell_{\text{VCVPF}} < \ell_{\text{VPF}} < \ell_{\text{exact}}$. Therefore, progressive waves are fully inhibited according to the viscous theories for $\ell < \ell_{\text{VCVPF}}$, whereas these theories agree and predict standing waves for $\ell > \ell_{\text{exact}}$. This tendency was also described in Figure 1. The transition values ℓ_c from the three theories become larger with increasing J as can be noted in Figure 13 for $J = 40$. In Figures 15 and 17 for $J = 500$ and $J = 10^{-6}$, respectively, the cross-over ℓ_c obtained from each viscous theory is larger than 100 and lie out of the figures. At least for values of $\ell << \ell_{\text{exact}}$ in the neighborhood of $\ell = 2$, VCVPF provides the better approximation of the decay rate. For large J, in the regime of progressive waves, the region of good agreement between VCVPF and the exact solution extends to higher values of ℓ (e.g., $2 \leq \ell \leq 100$ for $J = 10^{-6}$ in Figure 17), while VPF shows poor agreement in comparison.

Good agreement with the exact solution for the frequency of the oscillations is observed for low values of ℓ from the three approaches (i.e. VPF, VCVPF and IPF). For moderate to large values of J, the oscillatory regime appears for a certain ℓ interval starting with $\ell = 2$. This interval becomes wider as J increases. As J increases, the cross-over ℓ_c moves to the right and the agreement in terms of the frequency becomes much better in particular for low values of ℓ, for which VCVPF has the best performance. These results can be observed in Figures 14 and Figures 16 for $J = 40$ and $J =$ 500, respectively. On the other hand, since the cross over value ℓ_{VPF} is larger than ℓ_{VCVPF}, VPF follows the trend of the exact solution in the oscillatory regime for a wider interval. In Figures 12 and 14, the graph of frequency versus mode number depicts a maximum. This maximum lies beyond the interval of ℓ used in the figures for $J \geq 500$. For very large values of J, the three approximations cannot be distinguished from the predictions given by the exact solution for a wide ℓ interval (e.g., $2 \leq \ell \leq 100$ for $J = 10^{-6}$ in Figure 18). Therefore, one can expect a good approximation inasmuch as $\ell << \ell_c$. For very small values of J, as in the case of $J = 10^{-3}$, the exact solution, VPF and VCVPF predict monotonically decaying waves and thus zero frequency, while IPF is off the mark giving rise to a non-zero frequency for non-decaying waves (see Figure 10).

For a bubble, Figures 19 through 28 show results for the decay rate and frequency for several values of J ranging from $J = 10^{-3}$ to $J = 10^6$. To some extend, similar trends as those described for the drop are observed for the bubble. However, two noteworthy differences can be mentioned. Firstly, for low to moderate J (from 10^{-3} to 500), VPF predicts decay rates closer to the values from the exact solution than VCVPF (for instance, see Figures19 and 23). This trend is reversed for large J (e.g., see Figure 27). Secondly, the agreement in terms of the frequency between either VPF or IPF and the exact solution is not as good for low values of ℓ as in the case of the drop, for low and moderate values of J. Notice that when VPF predicts standing waves, this theory approaches very well the decay rate given by the exact solution for progressive waves with very low frequencies (Figures 19 and 21). Presumably, this trend is kept for greater values of J and large values of $\ell > \ell_{\text{VPF}}$.

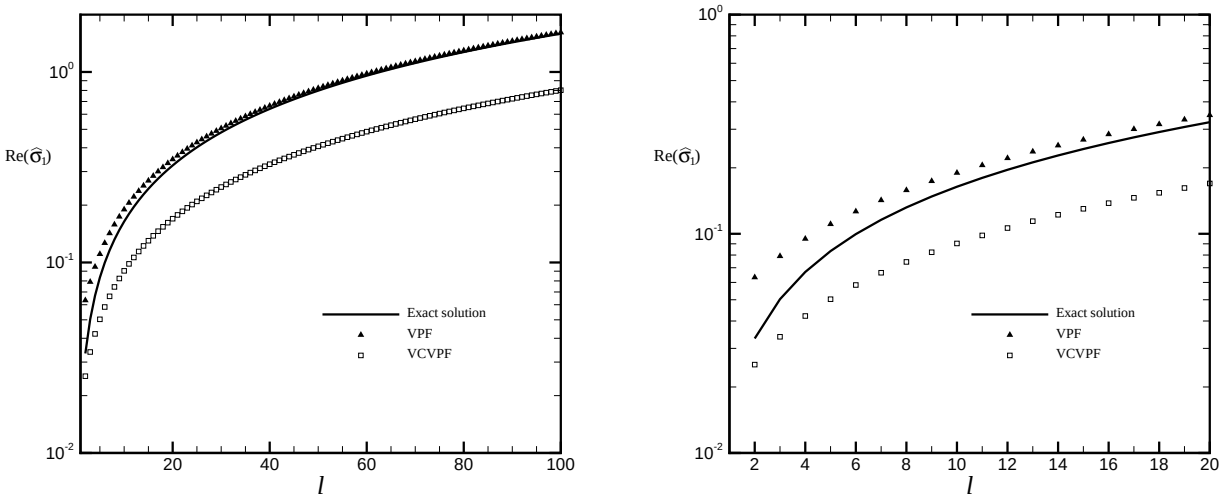

(a) wide spectrum (b) zoomed view

Figure 9: Decay rate $\mathrm{Re}(\hat{\sigma}_1)$ for $J = 10^{-3}$ versus the mode number ℓ for a *drop*. For the interval of ℓ shown, the eigenvalues are real and different. The lower decay rate (the most important from the physical point of view) is plotted. In (a) the full spectrum considered in this work is presented whereas in (b) the region of low values of ℓ is zoomed.

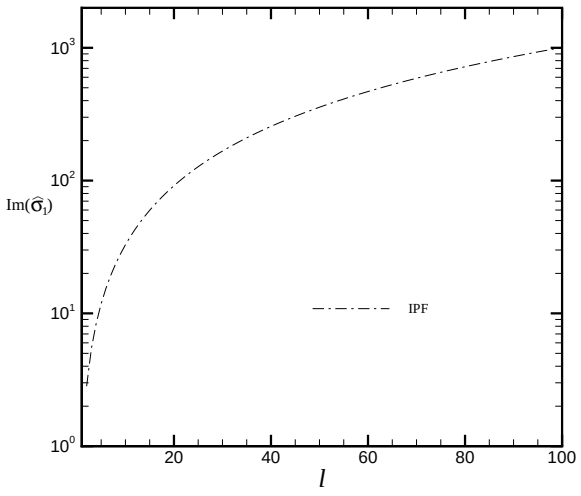

Figure 10: Wave frequency $\mathrm{Im}(\hat{\sigma}_1)$ for $J = 10^{-3}$ versus the mode number ℓ for a *drop*. For the interval of ℓ considered, the three theories VPF, VCVPF and the exact solution predict real eigenvalues. Therefore, the trend exhibited by $\mathrm{Im}(\hat{\sigma}_1)$ is only shown for IPF, which predicts oscillatory waves with constant amplitude.

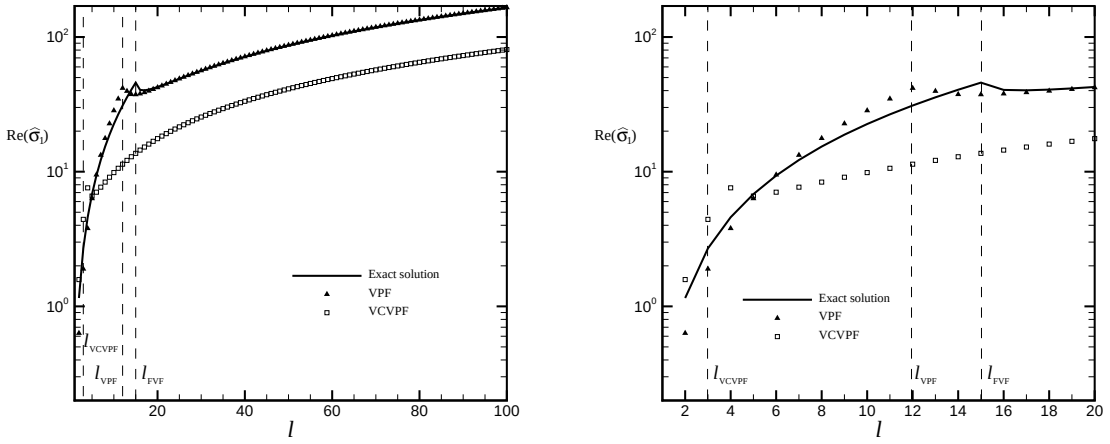

(a) wide spectrum (b) zoomed view

Figure 11: Decay rate $\mathrm{Re}(\hat{\sigma}_1)$ for $J = 10$ versus the mode number ℓ for a *drop*. In this case, the eigenvalues are a pair of complex conjugates for the interval of $\ell < \ell_c$ and they are real and different for $\ell \geq \ell_c$. For the latter case, the lower decay rate is plotted. The symbol ℓ_c stands for the highest value of ℓ for which a non-zero imaginary part is obtained, i.e. progressive waves occur. For instance, $\ell_{\mathrm{exact}} = \ell_c$ from fully viscous flow theory (exact solution); analogous definitions can be set for VPF (ℓ_{VPF}) and VCVPF (ℓ_{VCVPF}). In (a) the full spectrum considered in this work is presented whereas in (b) the region of low values of ℓ is zoomed.

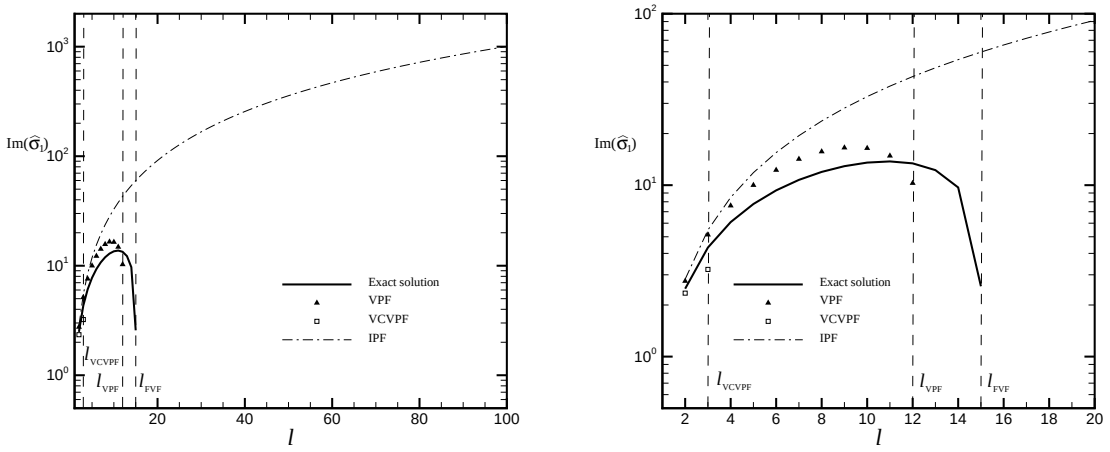

(a) wide spectrum (b) zoomed view

Figure 12: Wave frequency $\mathrm{Im}(\hat{\sigma}_1)$ for $J = 10$ versus the mode number ℓ for a *drop*. In this case, the eigenvalues are a pair of complex conjugates for the interval of $\ell < \ell_c$ and they are real and different for $\ell \geq \ell_c$. The symbol ℓ_c stands for the highest value of ℓ for which a non-zero imaginary part is obtained, i.e. progressive waves occur. For instance, $\ell_{\mathrm{exact}} = \ell_c$ from fully viscous flow theory (exact solution); analogous definitions can be set for VPF (ℓ_{VPF}) and VCVPF (ℓ_{VCVPF}). In (a) the full spectrum considered in this work is presented whereas in (b) the region of low values of ℓ is zoomed.

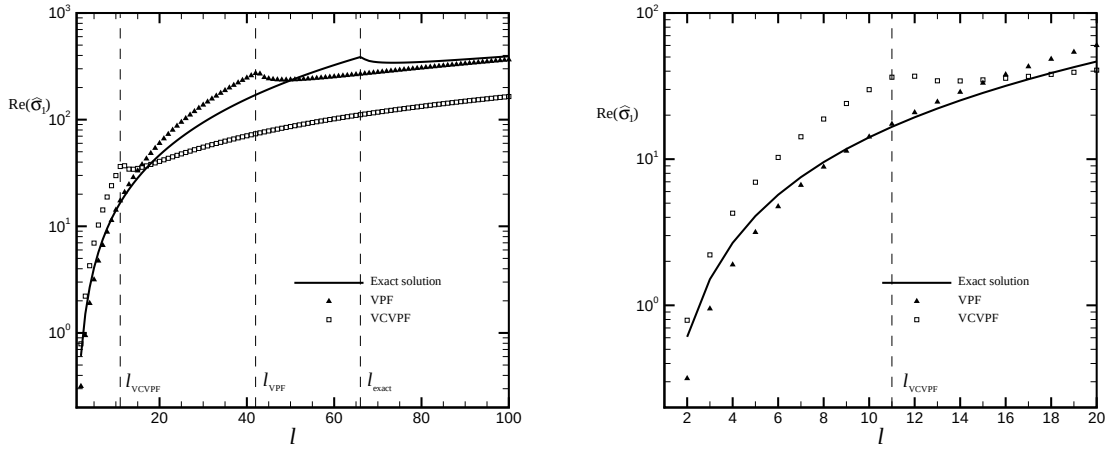

(a) wide spectrum (b) zoomed view

Figure 13: Decay rate $\mathrm{Re}(\hat{\sigma}_1)$ for $J = 40$ versus the mode number ℓ for a *drop*. In this case, the eigenvalues are a pair of complex conjugates for the interval of $\ell < \ell_c$ and they are real and different for $\ell \geq \ell_c$. For the latter case, the lower decay rate is plotted. The symbol ℓ_c stands for the highest value of ℓ for which a non-zero imaginary part is obtained, i.e. progressive waves occur. For instance, $\ell_{\mathrm{exact}} = \ell_c$ from fully viscous flow theory (exact solution); analogous definitions can be set or VPF (ℓ_{VPF}) and VCVPF (ℓ_{VCVPF}). In (a) the full spectrum considered in this work is presented whereas in (b) the region of low values of ℓ is zoomed.

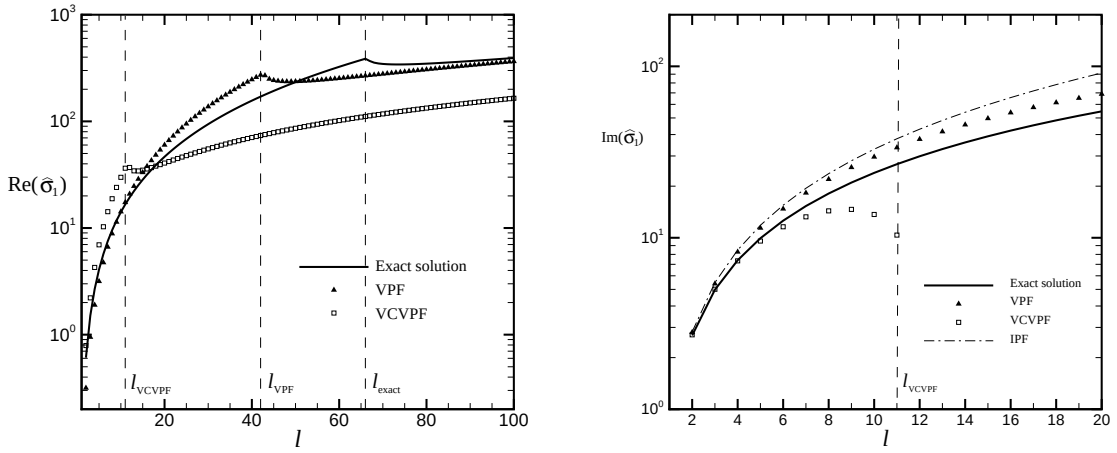

(a) wide spectrum (b) zoomed view

Figure 14: Wave frequency $\mathrm{Im}(\hat{\sigma}_1)$ for $J = 40$ versus the mode number ℓ for a *drop*. In this case, the eigenvalues are a pair of complex conjugates for the interval of $\ell < \ell_c$ and they are real and different for $\ell \geq \ell_c$. The symbol ℓ_c stands for the highest value of ℓ for which a non-zero imaginary part is obtained, i.e. progressive waves occur. For instance, $\ell_{\mathrm{exact}} = \ell_c$ from fully viscous flow theory (exact solution); analogous definitions can be set for VPF (ℓ_{VPF}) and VCVPF (ℓ_{VCVPF}). In (a) the full spectrum considered in this work is presented whereas in (b) the region of low values of ℓ is zoomed.

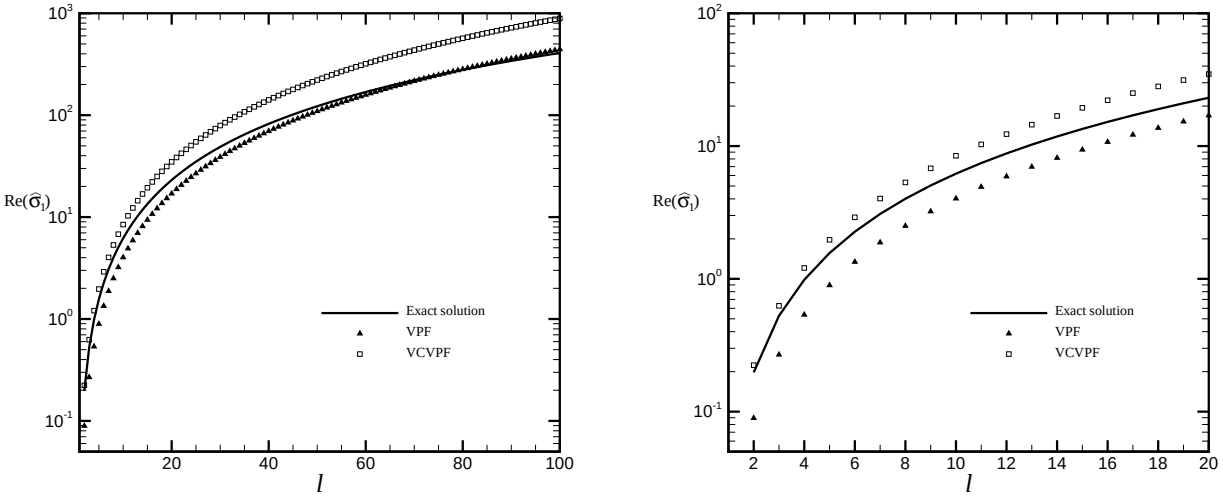

(a) wide spectrum (b) zoomed view

Figure 15: Decay rate $\mathrm{Re}(\hat{\sigma}_1)$ for $J = 500$ versus the mode number ℓ for a *drop*. In this case, the eigenvalues are a pair of complex conjugates for the interval of ℓ considered in this study. In (a) the full spectrum considered in this work is presented whereas in (b) the region of low values of ℓ is zoomed.

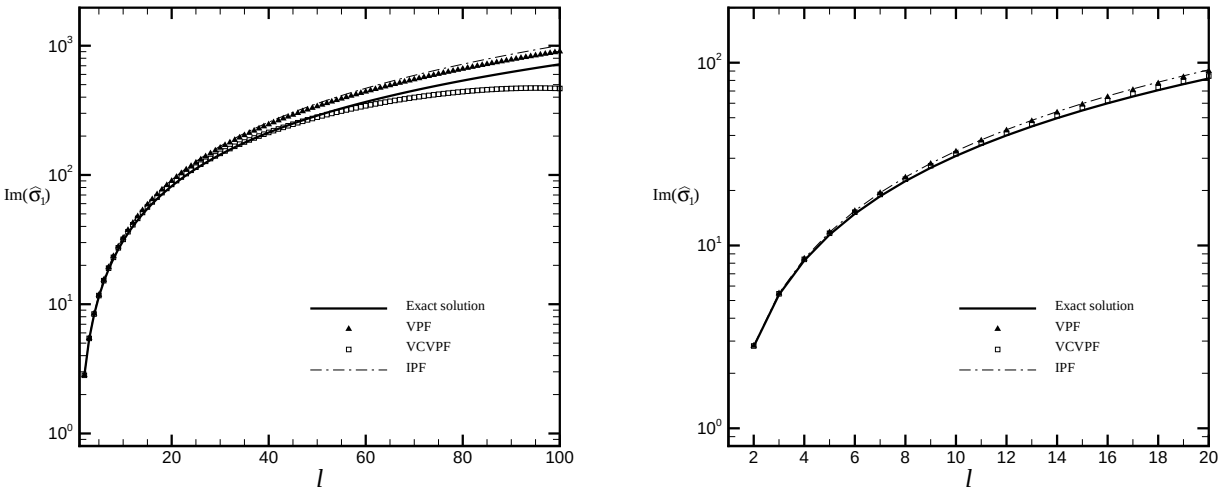

(a) wide spectrum (b) zoomed view

Figure 16: Wave frequency $\mathrm{Im}(\hat{\sigma}_1)$ for $J = 500$ versus the mode number ℓ for a *drop*. In this case, the eigenvalues are a pair of complex conjugates for the interval of ℓ considered in this study. In (a) the full spectrum considered in this work is presented whereas in (b) the region of low values of ℓ is zoomed.

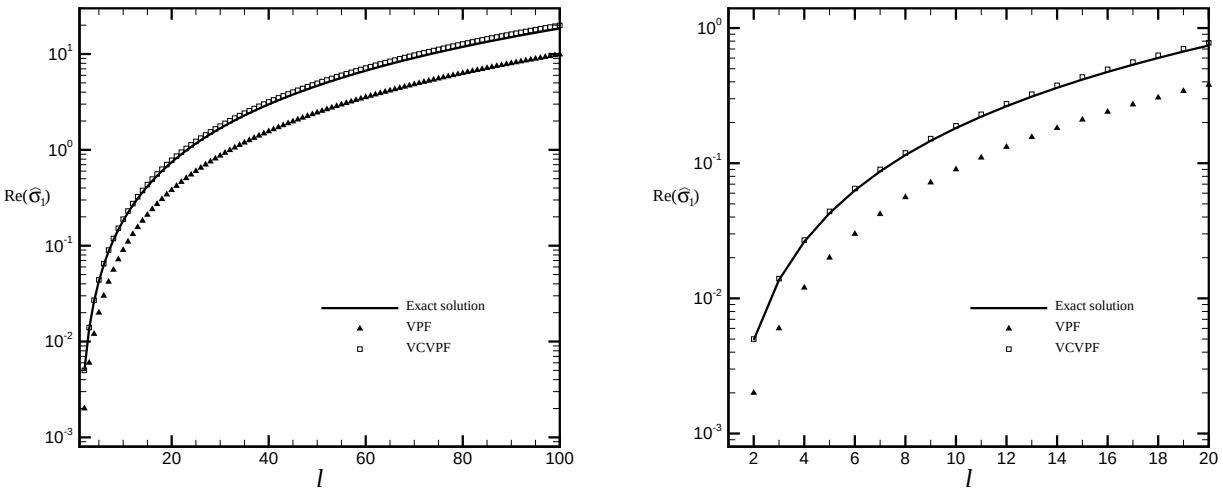

(a) wide spectrum (b) zoomed view

Figure 17: Decay rate $\mathrm{Re}(\hat{\sigma}_1)$ for $J = 10^6$ versus the mode number ℓ for a *drop*. In this case, the eigenvalues are a pair of complex conjugates for the interval of ℓ considered in this study. In (a) the full spectrum considered in this work is presented whereas in (b) the region of low values of ℓ is zoomed.

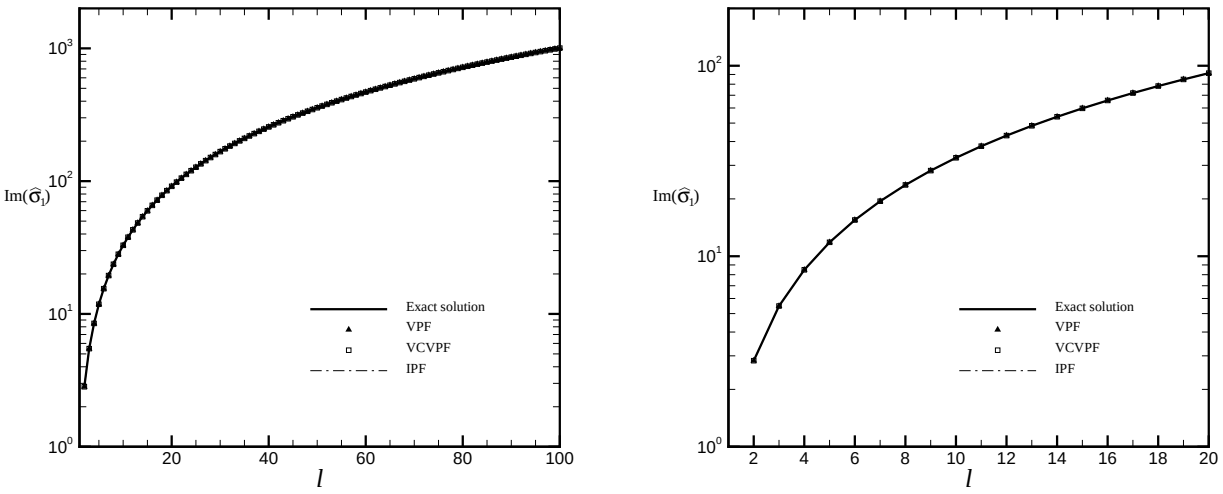

(a) wide spectrum (b) zoomed view

Figure 18: Wave frequency $\mathrm{Im}(\hat{\sigma}_1)$ for $J = 10^6$ versus the mode number ℓ for a *drop*. In this case, the eigenvalues are a pair of complex conjugates for the interval of ℓ considered in this study. In (a) the full spectrum considered in this work is presented whereas in (b) the region of low values of ℓ is zoomed.

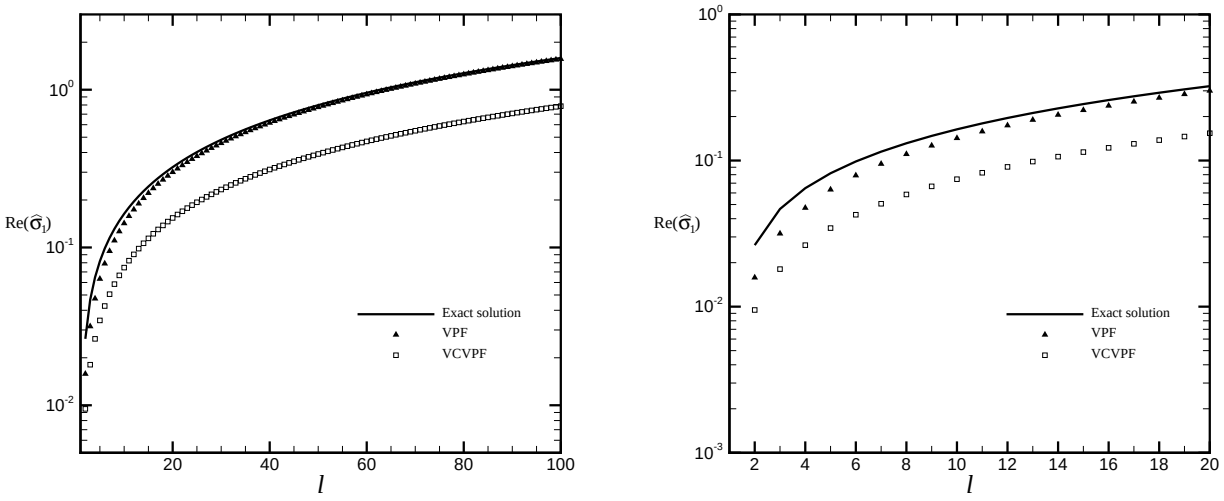

(a) wide spectrum (b) zoomed view

Figure 19: Decay rate $\mathrm{Re}(\hat{\sigma}_1)$ for $J = 10^{-3}$ vs. the mode number ℓ for a *bubble*. According to VPF and VCVPF, for the interval of ℓ considered, the eigenvalues are real and different. Here, the lower decay rate is plotted. From the exact solution, the eigenvalues are always complex, with non-zero imaginary part (i.e. progressive decaying waves). In (a) the full spectrum considered in this work is presented whereas in (b) the region of low values of ℓ is zoomed.

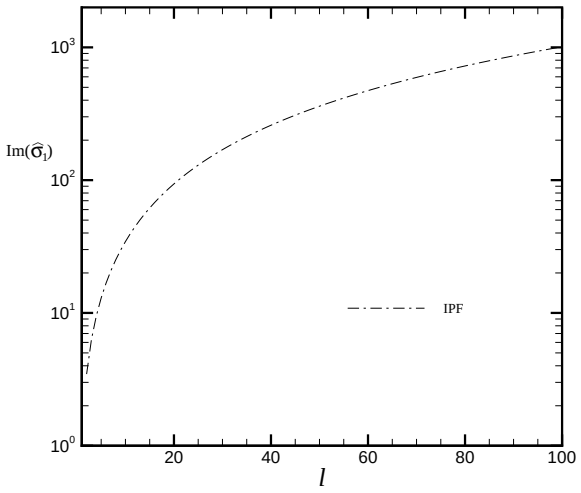

Figure 20: Wave frequency $\mathrm{Im}(\hat{\sigma}_1)$ for $J = 10^{-3}$ versus the mode number ℓ for a *bubble*. According to VPF and VCVPF, for the interval of ℓ considered, the eigenvalues are real and different. From the exact solution, the eigenvalues are always complex, with non-zero imaginary part (i.e. progressive decaying waves with a very long period of oscillation). Notice that $\mathrm{Im}(\hat{\sigma}_1)$ is much smaller than the corresponding value from IPF for any fixed ℓ; therefore, the exact solution predictions do not appear in the figure.

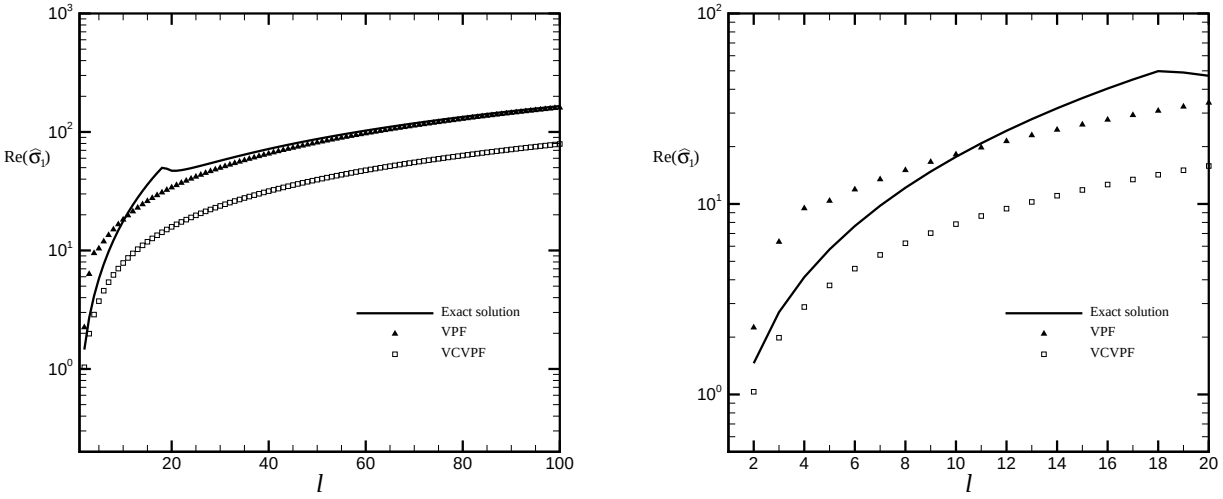

(a) wide spectrum (b) zoomed view

Figure 21: Decay rate $\mathrm{Re}(\hat{\sigma}_1)$ for $J = 10$ versus the mode number ℓ for a *bubble*. According to VPF and VCVPF, for the interval of ℓ considered, the eigenvalues are real and different. Here, the lower decay rate is plotted. From the exact solution, the eigenvalues are always complex, with non-zero imaginary part (i.e. progressive decaying waves). In (a) the full spectrum considered in this work is presented whereas in (b) the region of low values of ℓ is zoomed.

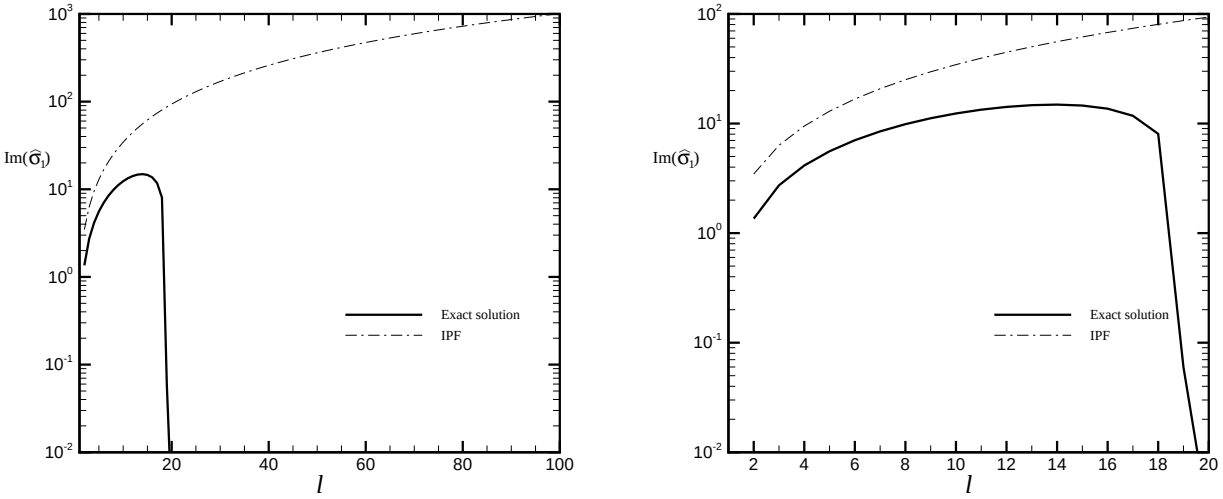

(a) wide spectrum (b) zoomed view

Figure 22: Wave frequency $\mathrm{Im}(\hat{\sigma}_1)$ for $J = 10$ versus the mode number ℓ for a *bubble*. According to VPF and VCVPF, for the interval of ℓ considered, the eigenvalues are real and different. From the exact solution, the eigenvalues are always complex, with non-zero imaginary part (i.e. progressive decaying waves). Notice that $\mathrm{Im}(\hat{\sigma}_1)$ approaches zero asymptotically as ℓ increases. In (a) the full spectrum considered in this work is presented whereas in (b) the region of low values of ℓ is zoomed.

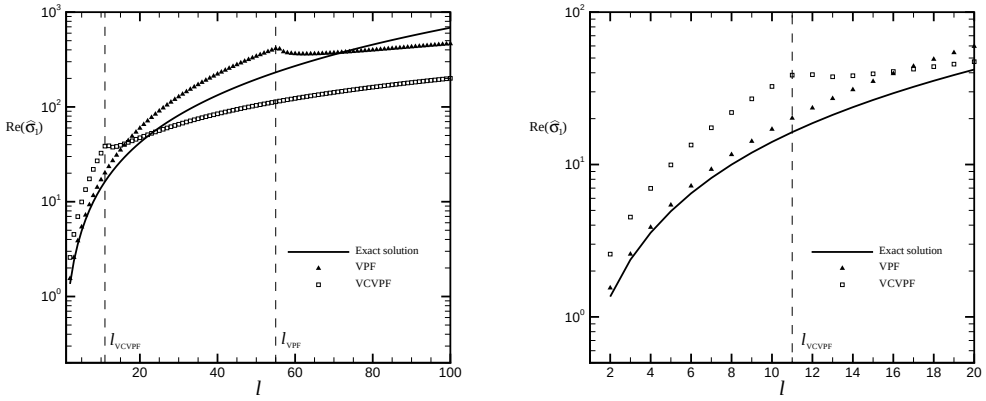

(a) wide spectrum (b) zoomed view

Figure 23: Decay rate $\mathrm{Re}(\hat{\sigma}_1)$ for $J = 60$ versus the mode number ℓ for a *bubble*. According to VPF and VCVPF, the eigenvalues are a pair of complex conjugates for the interval of $\ell < \ell_c$ and they are real and different for $\ell \geq \ell_c$. For the latter case, the lower decay rate is shown. From the exact solution, the eigenvalues are always complex, with non-zero imaginary part (i.e. progressive decaying waves). The symbol ℓ_c stands for the highest value of ℓ for which a non-zero imaginary part is obtained, i.e. progressive waves occur. For instance, $\ell_{\mathrm{VPF}} = \ell_c$ from VPF theory; analogous definitions can be set for VCVPF (ℓ_{VCVPF}). In (a) the full spectrum considered in this work is presented whereas in (b) the region of low values of ℓ is zoomed.

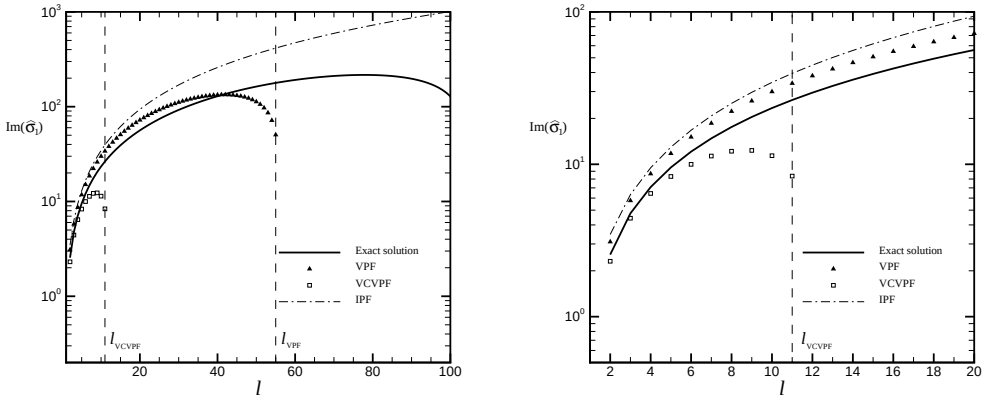

(a) wide spectrum (b) zoomed view

Figure 24: Wave frequency $\mathrm{Im}(\hat{\sigma}_1)$ for $J = 60$ versus the mode number ℓ for a *bubble*. According to VPF and VCVPF, the eigenvalues are a pair of complex conjugates for the interval of $\ell < \ell_c$ and they are real and different for $\ell \geq \ell_c$. From the exact solution, the eigenvalues are always complex, with non-zero imaginary part (i.e. progressive decaying waves). The symbol ℓ_c stands for the highest value of ℓ for which a non-zero imaginary part is obtained, i.e. progressive waves occur. For instance, $\ell_{\mathrm{VPF}} = \ell_c$ from VPF theory; analogous definitions can be set for VCVPF (ℓ_{VCVPF}). In (a) the full spectrum considered in this work is presented whereas in (b) the region of low values of ℓ is zoomed.

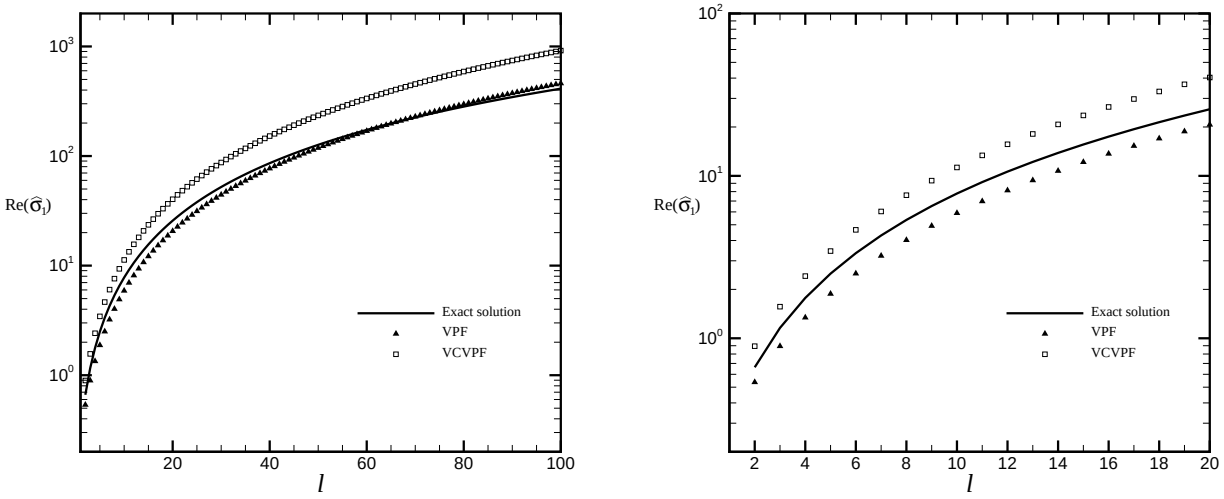

(a) wide spectrum (b) zoomed view

Figure 25: Decay rate $\mathrm{Re}(\hat{\sigma}_1)$ for $J = 500$ versus the mode number ℓ for a *bubble*. According to VPF and VCVPF, the eigenvalues are a pair of complex conjugates for the interval of ℓ considered in this study. From the exact solution, the eigenvalues are always complex, with non-zero imaginary part (i.e. progressive decaying waves). In (a) the full spectrum considered in this work is presented whereas in (b) the region of low values of ℓ is zoomed.

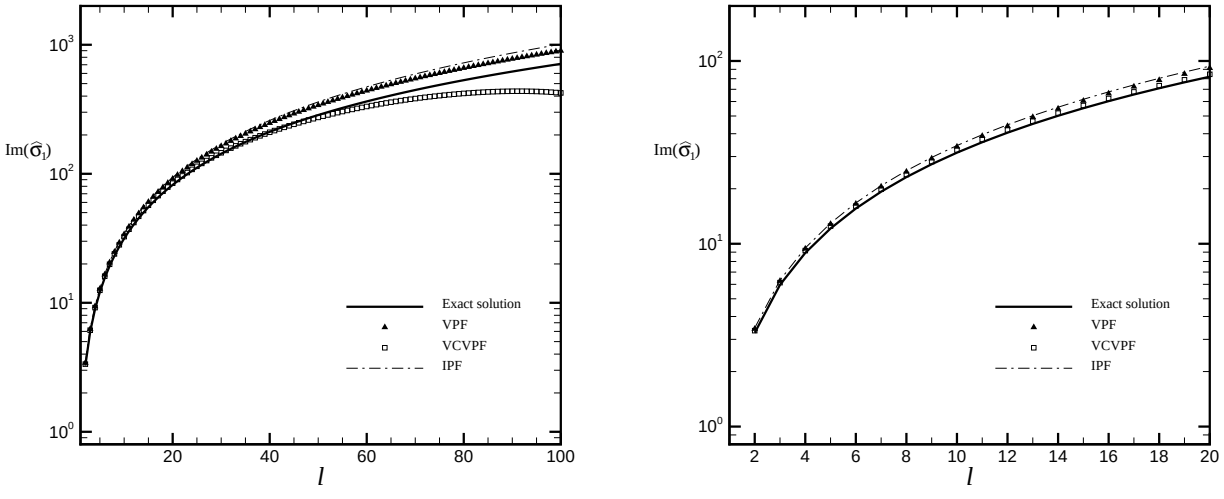

(a) wide spectrum (b) zoomed view

Figure 26: Wave frequency $\mathrm{Im}(\hat{\sigma}_1)$ for $J = 500$ versus the mode number ℓ for a *bubble*. According to VPF and VCVPF, the eigenvalues are a pair of complex conjugates for the interval of ℓ considered in this study. From the exact solution, the eigenvalues are always complex, with non-zero imaginary part (i.e. progressive decaying waves). In (a) the full spectrum considered in this work is presented whereas in (b) the region of low values of ℓ is zoomed.

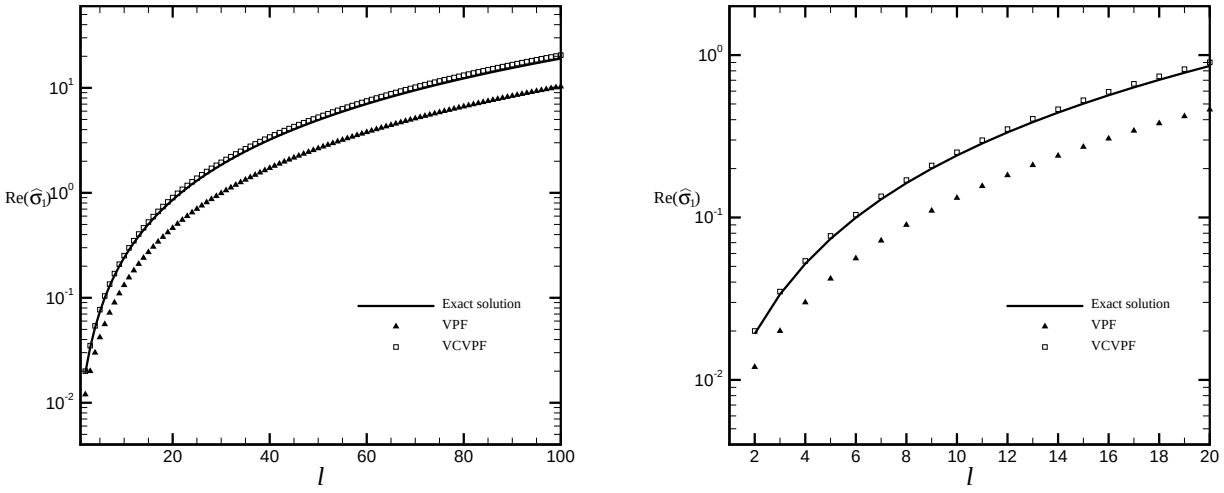

(a) wide spectrum (b) zoomed view

Figure 27: Decay rate $\mathrm{Re}(\hat{\sigma}_1)$ for $J = 10^6$ versus the mode number ℓ for a *bubble*. According to VPF and VCVPF, the eigenvalues are a pair of complex conjugates for the interval of ℓ considered in this study. From the exact solution, the eigenvalues are always complex, with non-zero imaginary part (i.e. progressive decaying waves). In (a) the full spectrum considered in this work is presented whereas in (b) the region of low values of ℓ is zoomed.

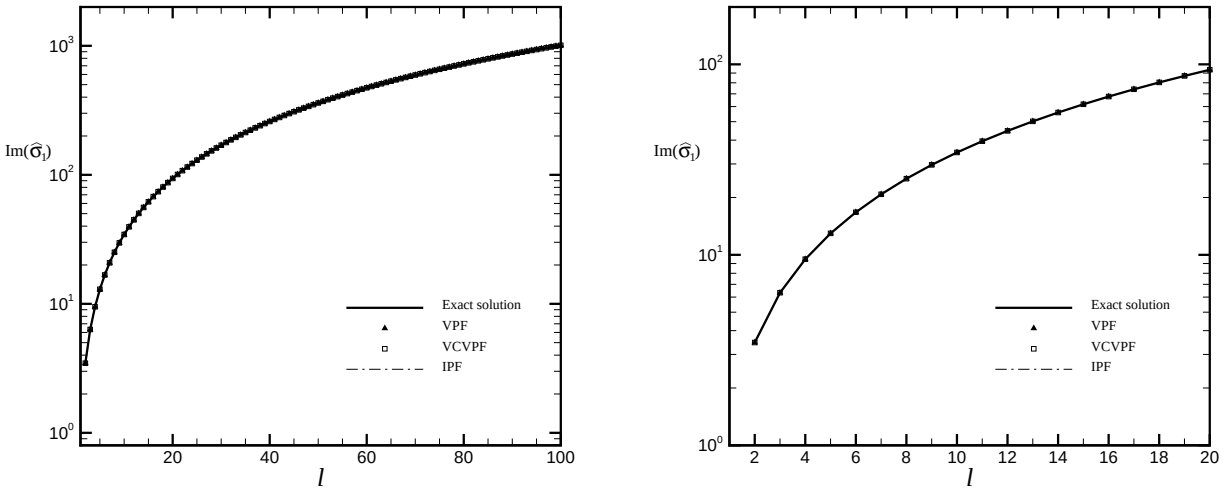

(a) wide spectrum (b) zoomed view

Figure 28: Wave frequency $\mathrm{Im}(\hat{\sigma}_1)$ for $J = 10^6$ versus the mode number ℓ for a *bubble*. According to VPF and VCVPF, the eigenvalues are a pair of complex conjugates for the interval of ℓ considered in this study. From the exact solution, the eigenvalues are always complex, with non-zero imaginary part (i.e. progressive decaying waves). In (a) the full spectrum considered in this work is presented whereas in (b) the region of low values of ℓ is zoomed.

Several figures showing the relative error between the predictions from the irrotational viscous theories VPF and VCVPF and those from the exact solution are shown in Appendix B for various Reynolds number J. The comparisons are carried out for the decay rate of the waves and the frequency of the progressive decaying waves for varying ℓ. In the latter case, IPF is also included in the comparison. The same performance and trends described in the previous paragraphs are appreciated in this Appendix from a different perspective.

Concluding remarks

This is the first study in which the machinery of irrotational theories of viscous flows is applied to the analysis of small perturbations of a spherical shape. The theory of viscous potential flow incorporates the effects of viscosity through the normal viscous stress at the interface. Since continuity of shear stresses and tangential velocities at the interface cannot be satisfied, in general, on a potential flow, VPF actually provides satisfactory results for problems with a gas-liquid interface in which the irrotational shear stress is zero or negligible. Examples of these problems are the Rayleigh-Poritsky bubble,'usually incorrectly attributed to Rayleigh-Plesset' (Joseph 2006), the rise of a spherical cap bubble and the Rayleigh-Taylor instability of either a viscous or viscoelastic fluid (Joseph, Belanger & Beavers 1999 and Joseph, Beavers & Funada 2002, respectively). The analysis of viscous potential flow is modified by adding a viscous pressure correction to the irrotational pressure that balances the difference between the irrotational shear stress and the true vanishingly small shear stress at the gas-liquid interface. This extra-pressure is determined by equating the power due to the pressure correction with the power of the irrotational shear stress.

The results obtained from the viscous purely irrotational approximations for the decay rate and frequency of the oscillations for a drop and a bubble are in good to reasonable agreement with the exact solution of the linearized problem. The damping role of viscosity in the dynamics of the waves is adequately described by the viscous irrotational theories through the modeling of the decay rate and frequency of the oscillations, whereas the classical inviscid theory predicts undamped oscillations, and thus, an identically-zero decay rate. Some features are noteworthy from the comparison carried out in this study for the drop and the bubble:

- In the limit of short waves (i.e., large mode number ℓ), VPF gives a very good approximation of the decay rate for standing waves for both the drop and the bubble. On the other hand, VCVPF gives rise to values of the decay rate in closer agreement with the exact solution within a certain ℓ interval, including $\ell = 2$, in the progressive waves regime (i.e. long waves) for large values of the Reynolds number J. In particular, for the fundamental mode, $\ell = 2$, and $J > O(10^3)$, the agreement is excellent in both cases, the drop and the bubble. This trend resembles the tendencies obtained for free gravity waves perturbing a plane interface by Wang & Joseph (2006). They found that VCVPF shows better agreement with the exact solution for long progressive waves while VPF gives rise to very good approximations for short standing waves. Nonetheless, a notable difference between their results and those given here is that surface tension has a stronger regularizing effect on short waves than gravity.

- VPF also follows the trend described by the exact solution for the frequency of the oscillations, since the transition from progressive to standing waves predicted by this irrotational theory occurs at a higher critical value of ℓ than the threshold given by VCVPF.

- The viscous irrotational approximations predict effects of viscosity on the frequency of the oscillations. For every mode, there is a Reynolds number J for which transition from progressive

waves to monotonically decaying waves occurs for either the drop or the bubble. Whereas a transitional value of J is predicted by the exact solution for a drop, only progressive waves are found by this theory for a bubble. In this case, very small frequencies are obtained as $J \to 0$ (e.g., $\nu \to \infty$).

- The viscous irrotational theories do not give rise to a continuos spectrum of eigenvalues for the bubble as has been found for the exact solution by Prosperetti (1980a).

In this study, we showed that the dissipation approximation yields the same dispersion relation and, thus, the same rate of decay and frequency of oscillations as VCVPF, as one can anticipate from previous works on different geometries. Indeed, the rate of decay of free gravity waves found by Lamb (1932) with the dissipation method was also obtained by Joseph & Wang (2004) using VCVPF. For the problem of capillary instability in which one of the fluids is of negligible density and viscosity and in the case of capillary instability involving two viscous liquids, Wang *et al.* (2005a, 2005b), respectively, found the same growth rate from the dissipation method and extra-pressure calculations. However, as mentioned by Wang *et al.* (2005a), the equivalence of the dissipation approximation and VCVPF is not guaranteed *a priori*, and so, it is verified after the calculation is carried out for a particular case. A proof on the equivalence of the two methods under a somewhat general framework is a task yet to be accomplished. Furthermore, the dissipation analysis presented by Lamb (1932) on the oscillations of drops and bubbles predicted viscous effects only on the rate of decay of the oscillation, whereas, the viscous irrotational theories used in the present study give rise to viscous effects in both the rate of decay and the frequency.

Acknowledgements

The work of J.C. Padrino and D.D. Joseph was partially supported by a grant 0302837 from the National Science Foundation.

References

[1] Basaran, O. 1992 Nonlinear oscillations of viscous liquid drops. *J. Fluid Mech.* **241**, 169–198.

[2] Bowman, J. J., Senior, T. B. A. & Uslenghi, P. L. E. (Ed.) 1987 *Electromagnetic and Acoustic Scattering by Simple Shapes.* Hemisphere Publishing Corporation, New York.

[3] Chandrasekhar, S. 1959 *The oscillations of a viscous liquid globe.* Proc. London Math. Soc. (3), 9, 141–49.

[4] Chandrasekhar, S. 1961 *Hydrodynamic and Hydromagnetic Stability.* Oxford University Press.

[5] Funada, T. & Joseph, D. D. 2002 Viscous potential flow analysis of capillary instability. *Int. J. Multiphase Flow* **28**, 1459–1478.

[6] Joseph, D. D. 2003 Viscous potential flow. *J. Fluid Mech.* **479**, 191–197.

[7] Joseph, D. D. 2006 Potential flow of viscous fluids: Historical notes. *Int. J. Multiphase Flow* **32**, 285–310.

[8] Joseph, D. D., Beavers, G.S. & Funada, T. 2002 Rayleigh–Taylor instability of viscoelastic drops at high Weber numbers. *J. Fluid Mech.* **453**, 109–132.

[9] Joseph, D. D., Belanger, J. & Beavers, G.S. 1999 Breakup of a liquid drop suddenly exposed to a high speed airstream. *Int. J. Multiphase Flow* **25**, 1263–1303.

[10] Joseph, D. D. & Liao, T.Y. 1994a Potential flows of viscous and viscoelastic fluids. *J. Fluid Mech.* **265**, 1–23.

[11] Joseph, D. D. & Liao, T.Y. 1994b Viscous and viscoelastic potential flow. In *Trends and Perspectives in Applied Mathematics.* vol. 100 (ed. S. Sirovich & V. Arnol'd) pp. 1–54. Springer.

[12] Joseph, D. D. & Wang, J. 2004 The dissipation approximation and viscous potential flow. *J. Fluid Mech.* **505**, 365–377.

[13] Lamb, H. 1881 On the oscillations of a viscous spheroid. *Proc. Lond. Math. Soc.* **13**, 51–66.

[14] Lamb, H. 1932 *Hydrodynamics.* Sixth edition. Cambridge University Press. Reprinted by Cambridge University Press, 1993.

[15] Lord Kelvin 1890 Oscillations of a liquid sphere, in *Mathematical and Physical Papers.* Clay and Sons, London, Vol. 3, pp. 384–386.

[16] Lord Rayleigh 1896 *The Theory of Sound.* Second edition. MacMillan, London. Reprinted by Dover, New York, 1945. Vol. 2, p. 371.

[17] Lundgren, T.S. & Mansour, N.N. 1988 Oscillations of drops in zero gravity with weak viscous effects. *J. Fluid Mech.* **194**, 479–510.

[18] Miller, C. A. & Scriven, L. E. 1968 The oscillations of a fluid droplet immersed in another fluid. *J. Fluid Mech.* **32**(3), 417–435.

[19] Moriguchi, K. W., Udagawa, K. & Hitotsumatsu, S. 1999 *Mathematical Formulae III.* Iwanami, 15th ed.

[20] Patzek, T.W., Benner, R.E., Basaran, O.A. & Scriven, L.E. 1991 Nonlinear oscillations of inviscid free drops. *J. Comp. Phys.* **97**, 489–515.

[21] Prosperetti, A. 1976 Viscous effects on small-amplitude surface waves. *Phys. Fluids* **19**, 2, 195–203.

[22] Prosperetti, A. 1977 Viscous effects on perturbed spherical flows. *Quart. Appl. Math.* **35**, 339–352.

[23] Prosperetti, A. 1980a Normal-mode analysis for the oscillations of a viscous liquid drop in an immiscible liquid. *J. Méc.* **19**, 1, 149–182.

[24] Prosperetti, A. 1980b Free oscillations of drops and bubbles: the initial value problem. *J. Fluid Mech.* **19**, 1, 149–182.

[25] Reid, W.H. 1960 The oscillations of a viscous liquid drop. *Quart. Appl. Math.* **18**, 86–89.

[26] Strauss, W. A. 1992 *Partial Differential Equations: An Introduction.* John Wiley & Sons, Inc.

[27] TOMOTIKA, S. 1935 On the stability of a cylindrical thread of a viscous liquid surrounded by another viscous fluid. *Proc. R. Soc. Lond.* A **150**, 322–337.

[28] TSAMOPOULOS, J.A. & BROWN, R.A. 1983 Nonlinear oscillations of inviscid drops and bubbles. *J. Fluid Mech.* **127**, 519–537.

[29] VALENTINE, R.S., SATHER, N.F. & HEIDEGER, W.J. 1965 The motion of drops in viscous media. *Chem. Eng. Sci.* **20**, 719–728.

[30] WANG, J., JOSEPH, D. D. & FUNADA, T. 2005a Pressure corrections for potential flow analysis of capillary instability of viscous fluids. *J. Fluid Mech.* **522**, 383–394.

[31] WANG, J., JOSEPH, D. D. & FUNADA, T. 2005b Viscous contributions to the pressure for potential flow analysis of capillary instability of two viscous fluids. *Phys. Fluids* **17**, 052105.

[32] WANG, J., & JOSEPH, D. D. 2006 Purely irrotational theories of the effect of the viscosity on the decay of free gravity waves. *J. Fluid Mech.* Accepted for publication.

A Integration formula

In the analysis presented in §3, §4 and §6 the following formula is invoked,

$$\int_A \left(B+\bar{B}\right)\left(C+\bar{C}\right)\mathrm{d}A = 2\int_A \mathrm{Re}\left[BC+B\bar{C}\right]\mathrm{d}A = 2\mathrm{Re}\left[\int_A \left(BC+B\bar{C}\right)\mathrm{d}A\right] \tag{A.3}$$

where A represents either a surface or a volume and B and C are complex fields. The bar indicates complex conjugate and $\mathrm{Re}\left[\cdot\right]$ is a linear operator that returns the real part of a complex number.

B Additional comparison of the irrotational approaches with the linearized fully viscous solution.

Figures 1 and 3 present a through comparison of the predictions from VPF and VCVPF with those from the exact solution for the rate of decay and frequency of the oscillatory waves, respectively, as function of ℓ for a wide range of the mode number ℓ in the case of the drop. The comparisons are carried out in terms of the relative error with respect to the exact solution results. In the case of the bubble, the same comparisons are shown in Figures 2 and 4. These plots provide additional support to the extensive comments presented in the discussion section analyzing and comparing the performance of the various irrotational approaches with the exact solution of the linearized problem.

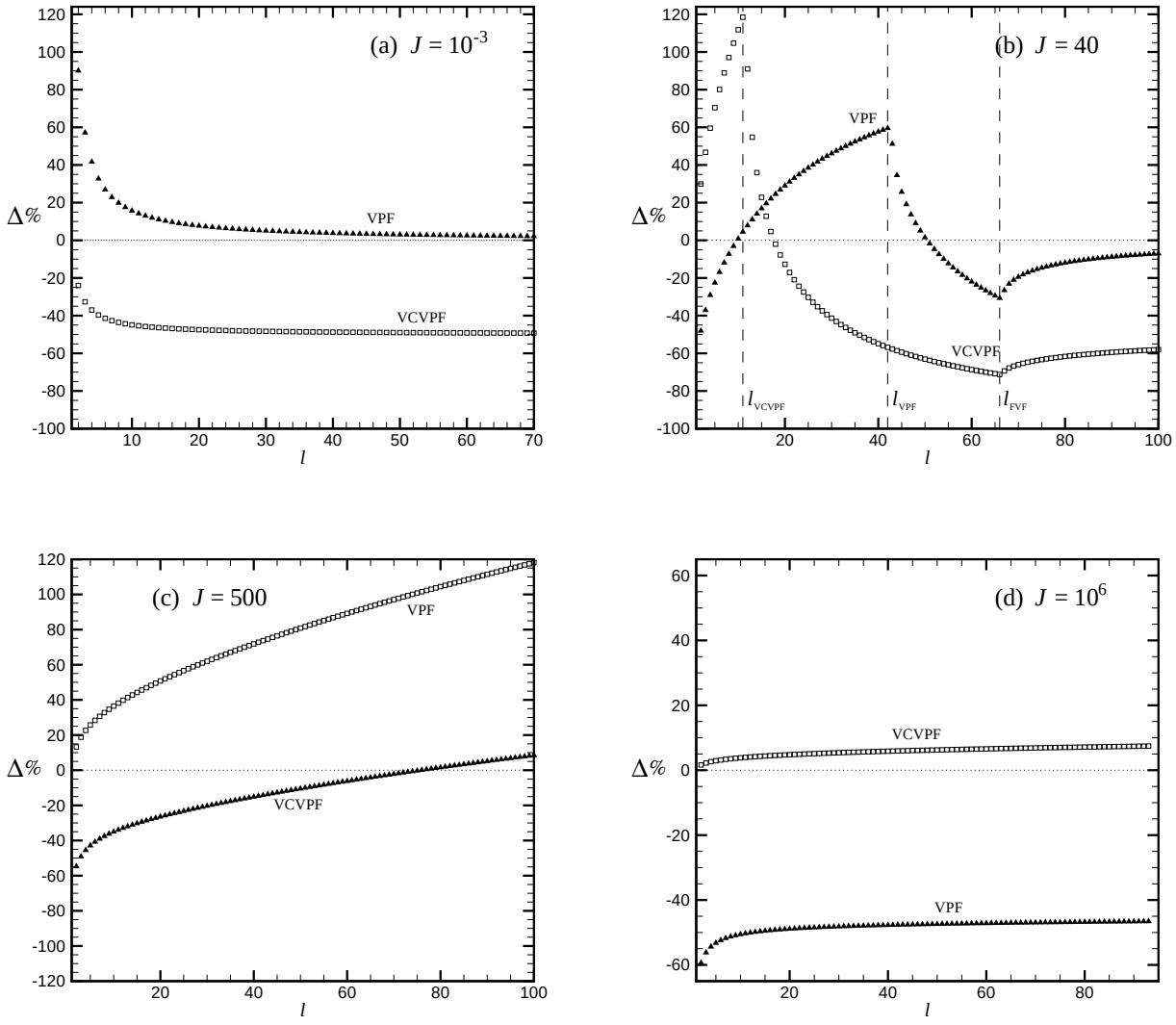

Figure 1: Relative error between the rate of decay predicted by either VPF or VCVPF with that predicted by the exact solution for a *drop* as a function of the mode number ℓ for four values of the Reynolds number J: (a) $J = 10^{-3}$; (b) $J = 40$; (c) $J = 500$; (d) $J = 10^6$. The relative error for a scalar Σ is computed as $\Delta\% = (\Sigma_{\rm VPF}/\Sigma_{\rm exact} - 1)\,100$; similar definitions stand for VCVPF and IPF. For these diagrams, Σ is replaced by the rate of the decay.

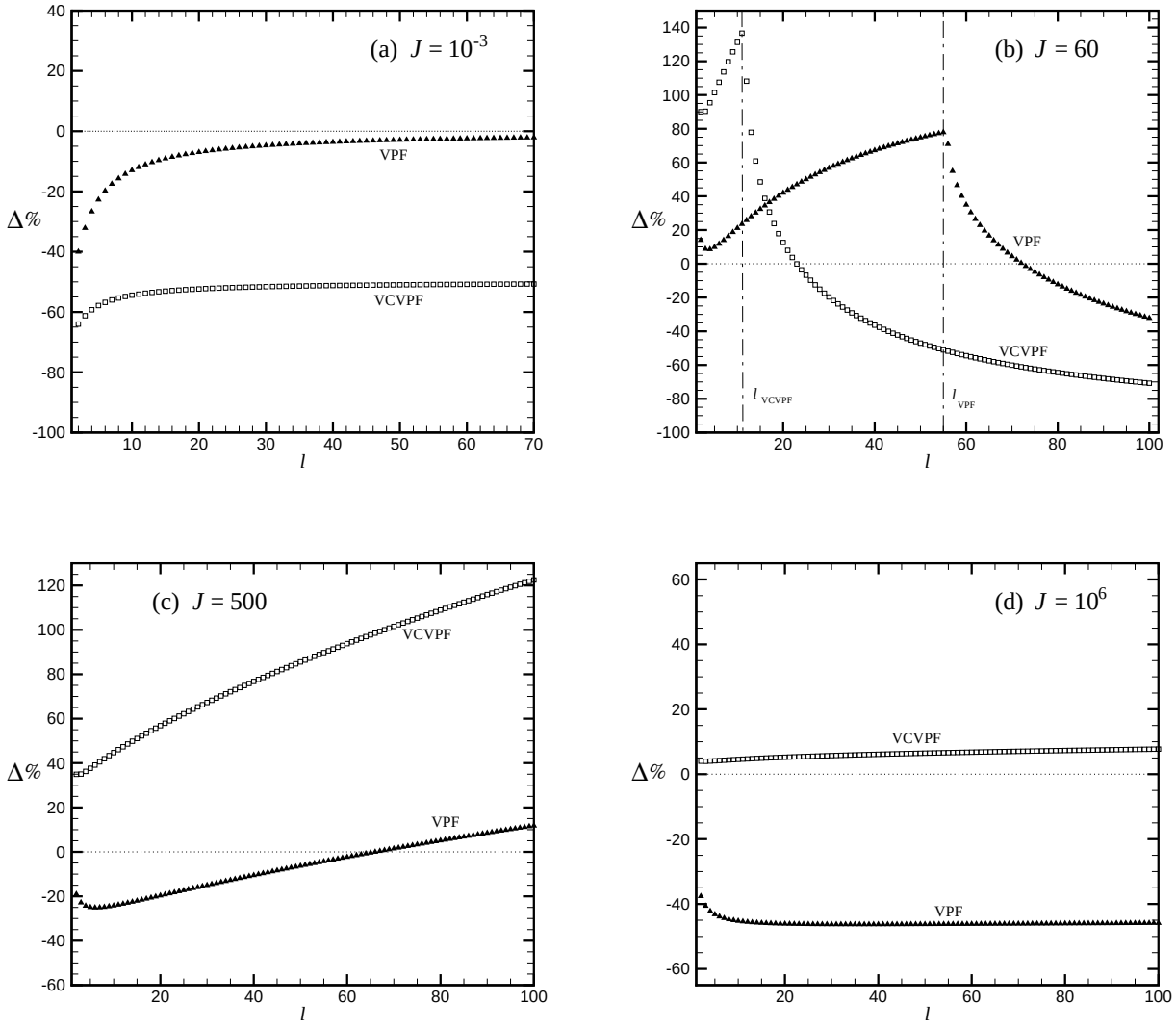

Figure 2: Relative error between the rate of decay predicted by either VPF or VCVPF with that predicted by the exact solution for a *bubble* as a function of the mode number ℓ for four values of the Reynolds number J: (a) $J = 10^{-3}$; (b) $J = 60$; (c) $J = 500$; (d) $J = 10^6$. The relative error for a scalar Σ is computed as $\Delta\% = (\Sigma_{\rm VPF}/\Sigma_{\rm exact} - 1)\,100$; similar definitions stand for VCVPF and IPF. For these diagrams, Σ is replaced by the rate of the decay.

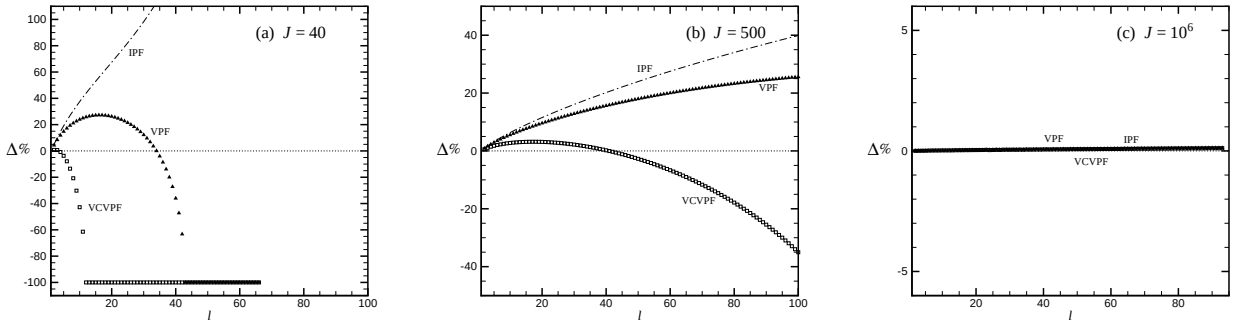

Figure 3: Relative error between the oscillation frequency predicted by either VPF, VCVPF or IPF with that predicted by the exact solution for a *drop* as a function of the mode number ℓ for three values of the Reynolds number (a) $J = 40$; (b) $J = 500$; (c) $J = 10^6$. The relative error for a scalar Σ is computed as $\Delta\% = (\Sigma_{\rm VPF}/\Sigma_{\rm exact} - 1)\, 100$; similar definitions stand for VCVPF and IPF. For these diagrams, Σ is replaced by the frequency. When either VPF or VCVPF predicts standing–decaying waves and the exact solution predicts progressive-decaying waves, $\Delta = -100\%$, as in figure (a).

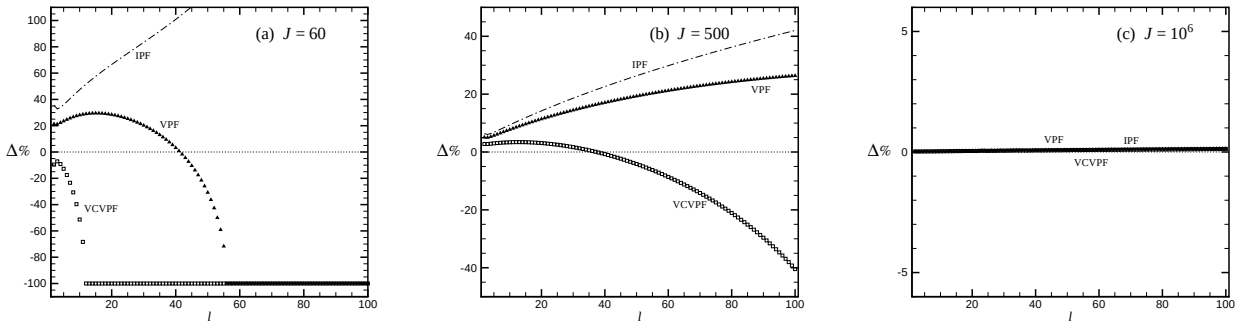

Figure 4: Relative error between the oscillation frequency predicted by either VPF, VCVPF or IPF with that predicted by the exact solution for a *bubble* as a function of the mode number ℓ for three values of the Reynolds number (a) $J = 60$; (b) $J = 500$; (c) $J = 10^6$. The relative error for a scalar Σ is computed as $\Delta\% = (\Sigma_{\rm VPF}/\Sigma_{\rm exact} - 1)\, 100$; similar definitions stand for VCVPF and IPF. For these diagrams, Σ is replaced by the frequency. When either VPF or VCVPF predicts standing–decaying waves, $\Delta = -100\%$, as in figure (a), since the exact solution always predicts progressive-decaying waves for the bubble.